A survey of interactions in crystal structures of pyrazine-based compounds

Fatemeh Taghipour and Masoud Mirzaei*

Department of Chemistry, Faculty of Science, Ferdowsi University of Mashhad, Mashhad, Iran. *Correspondence e-mail: mirzaeesh@um.ac.ir

The important role of pyrazine (pz) and its derivatives in fields such as biochemistry and pharmacology, as well as in the study of magnetic properties, is surveyed. Recognition of these properties without extensive investigations into their structural properties is not possible. This review summarizes interactions that exist between these organic compounds by themselves in the solid state, as well as those in coordination polymers with metal ions and in polyoxometalate-based hybrids. Complexes based on pyrazine ligands can generate metal–organic framework (MOF) structures that bind polyoxometalates (POMs) through covalent and noncovalent interactions. Some biological and magnetic properties involving these compounds are considered and the effect of hydrogen bonding on their supramolecular architectures is highlighted.

1. Introduction

Pyrazine is a weaker base compared to the other diazines (pyrimidine and pyridazine). These three molecules are rigid compounds which makes them ideal for the construction of metal–organic frameworks (MOFs) (Kumazawa *et al.*, 2003). MOFs are a subclass of coordination polymers with voids of different shapes and sizes whose study has seen rapid growth owing to various interesting applications (Rodenas *et al.*, 2015; Huang *et al.*, 2017; So *et al.*, 2015; Bai *et al.*, 2016; Giménez-Marqués *et al.*, 2016; Masih *et al.*, 2018). Whenever construction of MOF structures by covalent bonding has been reported, the importance of noncovalent interactions in the MOF architectures has been described infrequently (Manson *et al.*, 2006, 2007, 2009; Manson, Warter *et al.*, 2011). In order to test the ability of hydrogen bonding to create three-dimensional (3D) networks, it is important to prepare complexes with chemically flexible building-block units (such as pyrazine, which ligates easily with various paramagnetic metal ions) and ligands that can engage in very strong hydrogen-bonding interactions. Since the hydrogen bonds may link together magnetic centres in an intermolecular manner, it is interesting to understand the relationship between long-range and local structures for magnetic exchange pathways in low-dimensional coordination polymers and in MOFs that are linked by hydrogen-bonding interactions (Brown *et al.*, 2007). The functionalization of pyrazine units by electron-withdrawing or -donating groups, such as carboxylate, amine, amide *etc.*, provide opportunities for more interactions for the construction of structures with higher dimensions. In this respect, O—H···O, O—H···N and N—H···O hydrogen bonds, due to their strength and directionality, are frequently used to construct crystal structures. Weak hydrogen bonds, such as C—H···O and C—H···N, can also take part in the connectivity of supramolecular synthons and

feature articles
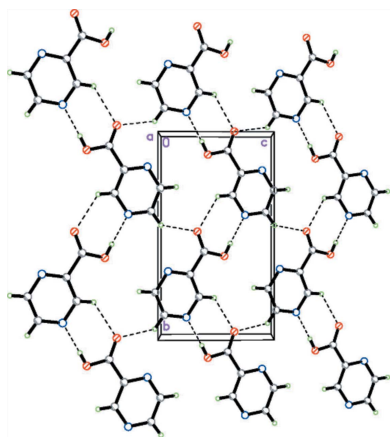
should not be discounted (Cockroft & Hunter, 2007; Rebek, 2005; Maurizot *et al.*, 2006; Rosen *et al.*, 2009; Bernstein *et al.*, 1995).

An interesting application of MOF structures is to provide a host for polyoxometalate (POM) units which might provide materials with interesting redox properties and because there are few high-dimensional structures of POM-based metal–organic frameworks (POMOFs) reported (Zhang *et al.*, 2018; Cheng *et al.*, 2018; Liu *et al.*, 2011), inclusion in this survey seems appropriate.

This review discusses how weak interactions between aggregating tectons based on pyrazine and its derivatives, with their varied donor and acceptor sites, induce different supramolecular assemblies that eventually result in the nucleation of a crystal. We discuss how hydrogen bonding can strengthen the crystal structures of pyrazine derivatives, including instances where the pyrazines are coordinated to metal centres. The investigation of chemical connectivity in the supramolecular structures of POM-based hybrids of pyrazine derivatives is interesting. By dividing the interactions between pyrazine-based MOFs and POM guests into covalent and noncovalent interactions, we can obtain knowledge about the directing forces that could be useful for crystal engineering in this class of compounds.

2. Pyrazine derivatives and their available donor–acceptor sites

The emphasis on structural studies of nitrogen-containing molecules, including pyrazine derivatives, is a result of various efforts that have been made in the synthesis of compounds having potential biological activity. Hence, in this section, the effect of some electron-withdrawing or -donating groups
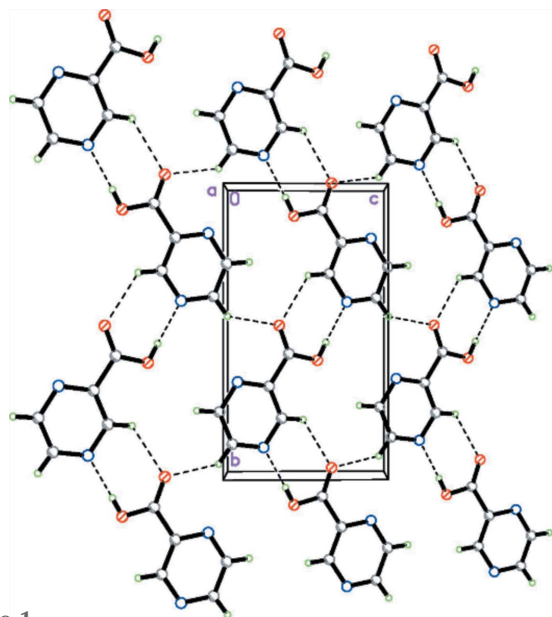

Figure 1
The 1D zigzag chains and 2D structure of pyrazine-2-carboxylic acid formed by O—H···N and C—H···O hydrogen bonds (dashed lines) between adjacent molecules. Reproduced from Shi *et al.* (2006) with permission.

containing O, N, S and halogen atoms on the stability of pyrazine derivatives is investigated. Moreover, how various types of intra- and intermolecular hydrogen bonding affect the interactions between fragments is also analyzed (Etter, 1990). Pyrazine and its methylated derivatives can use H atoms attached to sp^2- and sp^3-hybridized hydrocarbon groups for C—H···N hydrogen bonds and C—H···π interactions in the crystal packing. It is evident that sp^2-hybridized C—H groups have a greater acidity than sp^3-hybridized C—H units and it is expected that they should have a greater affinity for N atoms than for a π moiety. This behaviour has been investigated and it is observed that in an excess of any type of C—H donor in combination with pyrazine, trimethylpyrazine or tetramethylpyrazine, C—H···N interactions are the only ones observed. However, in dimethylpyrazine compounds, the stronger donors form C—H···N hydrogen bonds and the weaker donors are involved in C—H···π interactions. In addition, with increasing C—H acidity, the H···N distance decreases (Thalladi *et al.*, 2000). Pyridazine, as an isomer of pyrazine, is more basic and forms a layer structure in the crystal with intermolecular hydrogen bonding that involves four C—H groups of one molecule and the N atoms of adjacent fragments. The final structure is reinforced by π–π interactions (Podsiadło *et al.*, 2010). In the following section, the incorporation of O-donor moieties, such as carboxylate fragments, within the pyrazine skeleton and the resultant effect on the final crystal structures is described. Pyrazine N,N'-dioxide can exhibit enol and keto forms, and C—H···O hydrogen bonding involving the enol form is stronger than for the keto form. This leads to a planar structure, whereas the keto form exhibits a helical architecture (Näther *et al.*, 2002; Babu & Nangia, 2007). In planar pyrazine-2-carboxylic acid (2-pzc), one weak intramolecular hydrogen bond (C3—H3···O1) is observed and two intermolecular C—H···O hydrogen bonds with $R_2^2(7)$ motifs form zigzag one-dimensional (1D) chains which are coupled *via* C—H···O and π–π interactions into the final 3D structure (Fig. 1) (Shi *et al.*, 2006). This crystal structure presents a topology different from that reported previously for the orthorhombic polymorph (Takusagawa *et al.*, 1974).

The crystal structures of dihydrates of pyrazine-2,3-dicarboxylic acid (2,3-pzdc) have been reported several times (Ptasiewicz-Bąk & Leciejewicz, 1997a,b, 1998, 2003). The crystal structure of anhydrous pyrazine-2,3-dicarboxylic acid contains a network of hydrogen bonds that generate a layer assembly with planar pyrazine units (Premkumar *et al.*, 2004). In the 5-methylpyrazine-2,3-dicarboxylic acid crystal structure, intermolecular O—H···N hydrogen bonds form trimeric units that construct a helical assembly through C—H···O interactions. Interestingly, no π–π interactions between the layers were found (Babu & Nangia, 2006). Hydrogen bonding in some pyrazinecarboxylic acid derivatives [Scheme 1; reproduced from Vishweshwar *et al.* (2004) with permission] have been investigated and longer intermolecular O(acid)—H···O(water) hydrogen bonds were observed in **2**, **3** and **4** than in **1**, with two reasons given for this. First, due to the stronger hydrogen-bond donor ability of carboxylic acid
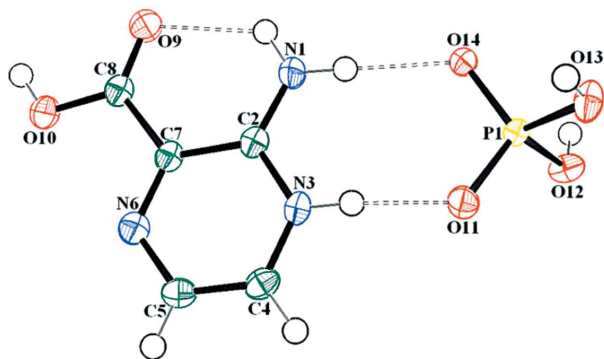
Figure 2
Schematic representation of the hydrogen bonds in 2-amino-3-carboxy-pyrazin-1-ium dihydrogen phosphate. Reproduced from Berrah *et al.* (2011) with permission.

compared to water and the presence of more electron-withdrawing groups in **1**, the role of σ-bond co-operativity is enhanced. Furthermore, polarization of the water molecules could cause a shortening of the hydrogen bonding in **1**. A remarkable result is seen in triacid **5**, where the O(acid)—H···O(water) hydrogen bonding is shorter than in **1** and is attributed to a stronger polarization-assisted hydrogen bonding in the water molecules in **5** (Vishweshwar *et al.*, 2004).

According to our results presented below, the introduction of N-donor fragments into pyrazine derivatives is expected to provide more stability to the final architectures than for the pyrazine system itself. 2,6-Diamino-3,5-dinitropyrazine and 2,6-diamino-3,5-dinitropyrazine 1-oxide take part in extensive intra- and intermolecular hydrogen-bonding interactions which construct two-dimensional (2D) graphite-like sheets (Gilardi & Butcher, 2001*a*). The presence of dimethyl sulfoxide (DMSO) in the lattice of 2,6-diamino-3,5-dinitropyrazine, by changing the nature of the interaction towards weaker C—H···O interactions, leads to a less compact packing arrangement (Gilardi & Butcher, 2001*b*). In the 2D network of the 2-amino-3-carboxypyrazin-1-ium dihydrogen phosphate salt, O—H···O hydrogen bonding creates a double-chain structure of anions. Intermolecular N—H···O and O—H···O hydrogen bonds connect cations and anions,

with the pyrazinium cation having an intramolecular N—H···O hydrogen bond (Fig. 2) (Berrah *et al.*, 2011).

Pyrazinamide and its derivatives are a subclass of pyrazine compounds for which many crystal structures have been determined. In these structures, the presence of various donor–acceptor groups, in combination with rigidity (or flexibility) of the molecules, may lead to different architectures. *N*-(3-Bromophenyl)pyrazine-2-carboxamide, due to its flexibility, can participate in a variety of interactions and forms tetrameric and dimeric polymorphs by halogen or hydrogen bonding (Fig. 3). In polymorph I, in addition to halogen bonding, intra- and intermolecular hydrogen bonds are found which have comparable bond lengths (Khavasi & Tehrani, 2013).
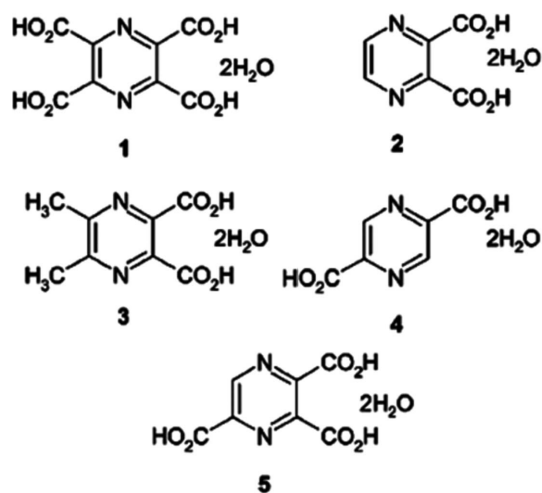
Scheme 1

A comparison of the structures of *N*-(4-halophenyl)pyrazine-2-carboxamide and *N*-(5-halo-2-pyridinyl)pyrazine-2-carboxamide suggests that the intramolecular N—H···N(py) (py is pyridine) hydrogen-bonding interaction generates better coplanarity between the aromatic rings (Khavasi *et al.*, 2014). In 6-fluoro-3-hydroxypyrazine-2-carboxamide, intramolecular O—H···O hydrogen bonding, in addition to preventing keto–enol tautomerism of the hydroxy group, forms a six-membered ring motif. Other hydrogen-bond and
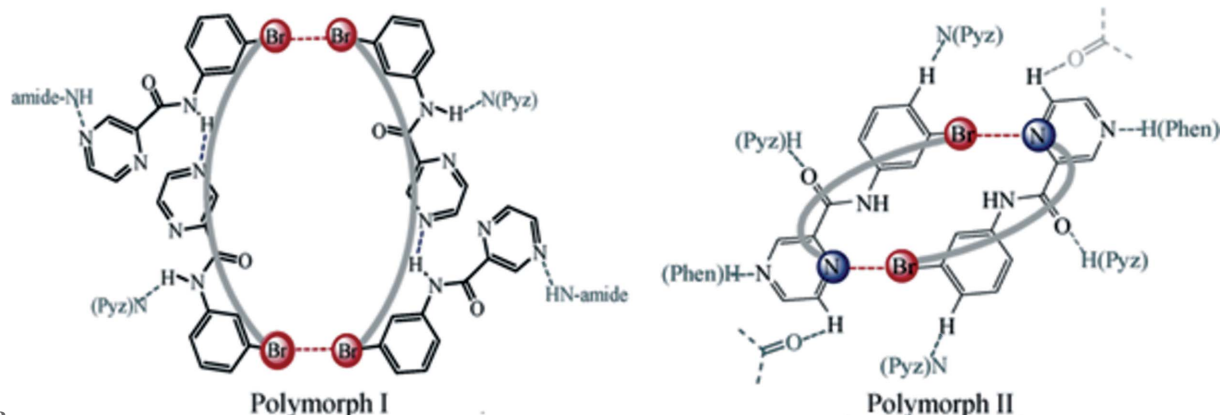

Figure 3
The tetrameric halogen/hydrogen-bonded synthon in polymorph I and the dimeric halogen-bonded synthon in polymorph II of *N*-(3-bromophenyl)pyrazine-2-carboxamide. Reproduced from Khavasi & Tehrani (2013) with permission.
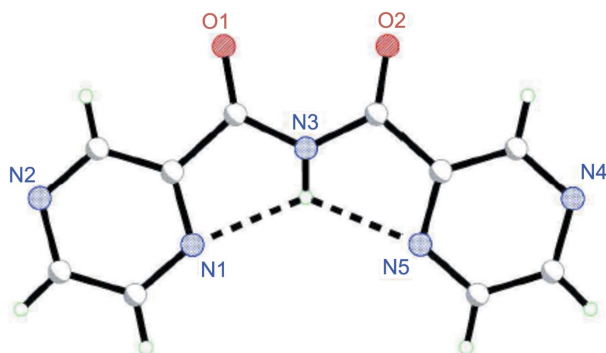
feature articles

Figure 4
The structure of the metal-free ligand Hdpzca and its intramolecular hydrogen bonding. Note the planarity of the entire ligand. Reproduced from Cowan *et al.* (2015) with permission.

π–π stacking interactions contribute to the stabilization of the network (Shi *et al.*, 2014). *N*-(Pyrazine-2-carbonyl)pyrazine-2-carboxamide (Hdpzca) as a symmetric pyrazine imide with various available donor–acceptor sites has the ability to construct 1D, 2D and 3D supramolecular assemblies. The near planarity of this molecule is the result of a fully conjugated π-system and the bifurcated intramolecular hydrogen-bonding interaction between imide atom H3*X* and pyrazine atoms N1 and N5 [N3$\cdots$N1 = 2.636 (4) Å and N3$\cdots$H3*X*$\cdots$N1 = 111.9°; N3$\cdots$N5 = 2.631 (4) Å and N3$\cdots$H3*X*$\cdots$N5 = 111.9°] (Fig. 4) (Cowan *et al.*, 2015).

The use of pyrazines with flexible side chains can generate interesting structural properties because having atoms such as N, O and S in the substituents increases the reactivity by introducing more sites for intermolecular interactions in the crystal. 1,10-Bis(pyrazinyl-2-carbonyl)-1,4,7,10-tetraazadecane
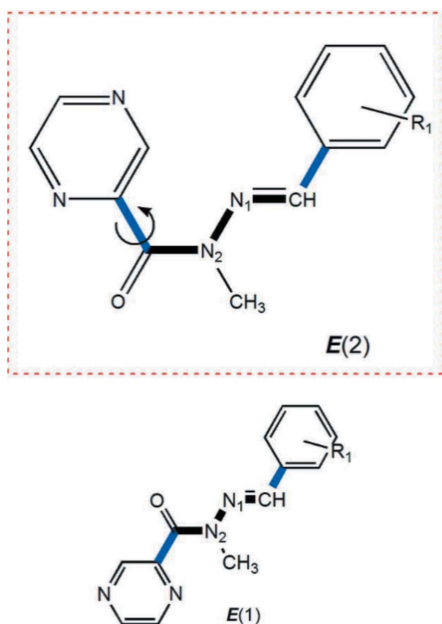

Figure 5
The conformations of *N'*-[(*E*)-aryl]pyrazine-2-carbohydrazides, where *E*(1) and *E*(2) are the *trans* and *cis* arrangements of the C=O and N2—CH₃ bonds, respectively. Reproduced from Gomes *et al.* (2013) with permission.

as a soft pyrazine ligand has available donor–acceptor sites and, in the presence of water molecules, acts as a host accommodating a six-membered ring of guest water molecules with four hydrogen bonds *via* carbonyl and nitrogen moieties (Shi & Zhang, 2007).

The arrangement of (*E*)-2-acetylpyrazine 4-nitrophenyl-hydrazone in the crystal is such that in addition to N—H$\cdots$N and C—H$\cdots$O hydrogen bonding, there is π–π stacking between parallel arene [3.413 (14) Å] and pyrazine [3.430 (8) Å] rings that are arranged face-to-face (Shan *et al.*, 2008). In the crystal structures of a series of (pyrazine-carbonyl)hydrazone monohalobenzaldehyde derivatives, *i.e.* $N_2C_4H_3CONHN{=}CHC_6H_4X$ (*X* = F, Cl or Br), intramolecular N—H$\cdots$O hydrogen bonding is observed with $D\cdots A$ separations ranging from 2.658 (5) Å for *X* = *m*-Br to 2.719 (4) Å for *X* = *o*-F, which block intermolecular hydrogen bonding *via* the N atom of the pyrazine units. In the *X* = *o*-Cl structure, in addition to incorporating N—H$\cdots$O hydrogen bonding, a C—H$\cdots$O hydrogen bond is formed between the pyrazine ring and the amide group of a neighbouring molecule. The intermolecular C—H$\cdots$O hydrogen bonding generates a ribbon-like structure that leads to π-stacking between the layers and the final 3D structure (Baddeley *et al.*, 2009).
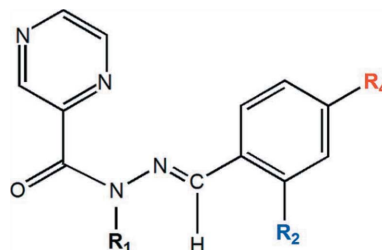
(I*b*) R₁=R₄= H; R₂= OCH₃
(I*c*) R₁=R₂= H; R₄= CN
(I*d*) R₁=R₄= H; R₂= NO₂

(II*a*) R₁= CH₃; R₂=R₄=H
(II*b*) R₁= CH₃; R₄= H; R₂= OCH₃
(II*c*) R₁= CH₃; R₂= H; R₄= CN
(II*d*) R₁= CH₃; R₄= H; R₂= NO₂
(II*e*) R₁= CH₃; R₂= H; R₄= NO₂

Scheme 2

Pyrazine-2-carbohydrazides have moderate antituberculosis properties but the methylated pyrazine-2-carbohydrazide derivatives do not. Therefore, comparisons between their structures may help in the understanding of the structure/activity relationships. In (I) [Scheme 2; reproduced from de Souza *et al.* (2011) with permission], hyperconjugation from the heteroaryl ring to the arene ring through the hydrazine unit has been suggested as the main contributor to the near planarity of type I compounds and this is reinforced by an intramolecular N—H$\cdots$N hydrogen bond. However, substitution of a methyl group on the N2 atom in the pyrazine-2-carbohydrazide system and the resulting intramolecular C—H$\cdots$O hydrogen bond between methyl and carbonyl groups changes the conformation so that the molecule is no longer

planar overall. It is thus suggested that the antitubercular properties of (I) could be attributed to the planarity of the molecules (Fig. 5) (Gomes *et al.*, 2013).

The incorporation of substituents that contain an S atom can play important roles in the stabilization of the crystal structures. The crystal structure of *S*-methyl 5-methylpyrazine-2-carbothioate and its solid-state interactions have been reported (Aubert *et al.*, 2007). This molecule has three types of intermolecular hydrogen-bonding interactions (two C—H···N and one C—H···O), as well as π-stacking interactions that generate the 3D crystal structure. Although the presence of the S atom does not have an important structure-directing effect in the crystal structure of this compound, this molecule can act as an intermediate in the preparation of various compounds of biological interest (Aubert *et al.*, 2007). The structures of three thio(semi)carbazones derived from 2-acetylpyrazine segments show various conformations and configurations depending on the arrangements of the molecular components. As there are several available donor–acceptor sites, intra- and intermolecular hydrogen-bonding networks in the crystal structures can be expected. Indeed, in *syn*-(1*E*)-2-acetylpyrazine-3-thiosemicarbazone (Fig. 6*a*), the H atom on N4 is involved in three types of interactions: (i) intramolecular hydrogen bonding with N1; (ii) intermolecular hydrogen bonding with the N atom of the pyrazine ring and the formation of dimers with an $R_2^2(18)$ ring pattern; (iii) interaction with the thioureide group of an adjacent molecule. The C—H···N(pz) and N2—H···S interactions connect fragments and lead to the overall 3D structure. In *syn*-(1*E*,4*Z*)-2-acetylpyrazine-4-ethyl-3-thiosemicarbazone (Fig. 6*b*), the thioureide groups interact with the pyrazine ring of an adjacent molecule in the mean molecular plane through two adjacent N2—H···N(pz) [2.401 (3) Å] and C—H···S [2.894 (3) Å] hydrogen bonds, while N4—H···N1 is an intramolecular interaction. In *syn*-(1*Z*)-2-acetylpyrazine-4,4-dimethyl-3-thiosemicarbazone, the pyrazine-ring configuration is such that the N atom of the pyrazine ring is *syn* to the N1—H bond and an intramolecular hydrogen bond is formed between them. The pyrazine ring also forms C—H···S hydrogen bonds

generating $R_2^2(20)$ graph sets (Fig. 6*c*) (Venkatraman *et al.*, 2009). In conclusion, the presence of different functional groups in pyrazine-based structures results in the formation of different hydrogen bonds with different strengths that are relevant in crystal engineering.

3. Pyrazine as a potent ligand in coordination polymers

Pillared layer structures are appropriate candidates for the construction of porous 3D networks (Russell *et al.*, 1997). While hydrogen-bonding interactions reinforce these structures, it is observed that in the absence of guest fragments, the structures lose their stability. Therefore, introduction of metal centres leads to more stable coordination networks (Zimmerman, 1997). Hence, despite the effective role of metal centres in coordination polymers, hydrogen bonds continue to have a prominent role in increasing the dimensions of the structures. This role was investigated in the crystal structures of complexes containing pyrazine derivatives. Complexes of pyrazine-2,3-dicarboxylic acid and transition-metal ions (TMs) display various architectures. In the 1:2 complex, monometallic [Ni(2,3-pzdcH)$_2$(H$_2$O)$_2$] units participate in a hydrogen-bonding network and, in addition to strong intramolecular hydrogen bonding among carboxylate groups [O—H···O = 2.408 (2) Å], display hydrogen bonding between coordinated water and neighbouring fragments to form a stable 3D structure. By contrast, [Cu(2,3-pzdcH)$_2$]$_x$·2H$_2$O adopts a chain structure with double-bridging 2,3-pzdc units that are fortified by hydrogen bonding of the lattice water molecules. The monomethyl ester of 2,3-pzdc coordinates differently with Cu cations and this changes the final architecture of the crystal. Here, one O atom and its adjacent N atom chelate in equatorial positions, while an uncoordinated O atom of another ligand occupies an axial position. With the ester groups uncoordinated, only a 2D polymer is generated (Neels *et al.*, 1997). In the case of 1:1 complexes, a 1D linear material is formed in which 2,3-pzdc acts as a tetradentate ligand to link to metal centres by coordinating in equatorial sites, with the axial positions occupied by H$_2$O molecules
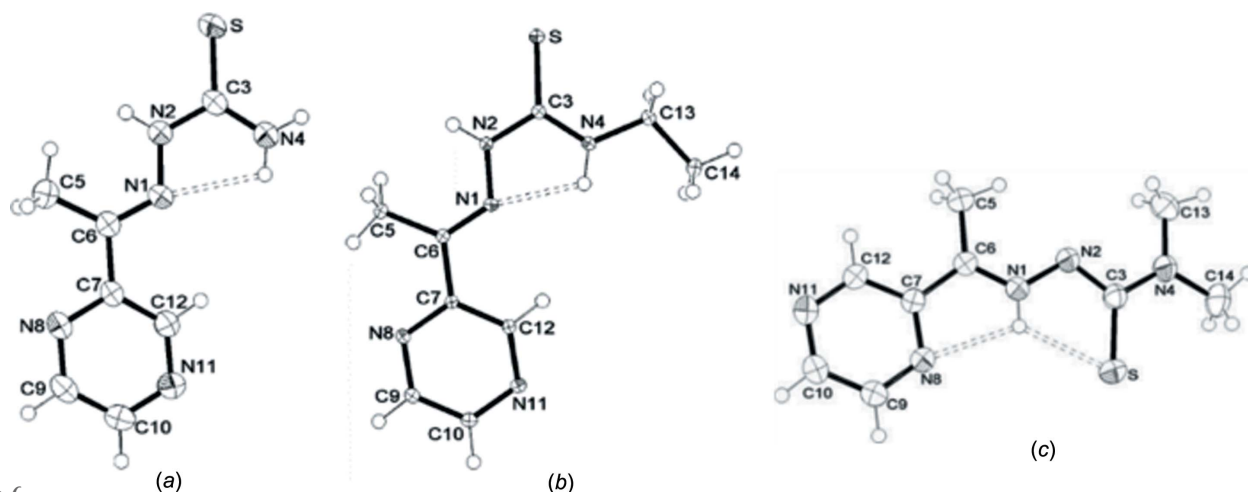

Figure 6
Displacement ellipsoid plots (50% probability) of three thiosemicarbazones. Reproduced from Venkatraman *et al.* (2009) with permission.
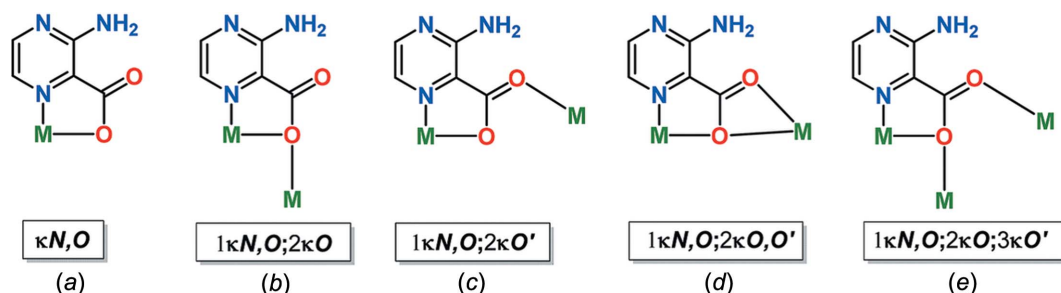
Figure 7
Schematic representation of the various coordination modes of 3-aminopyrazine-2-carboxylate. Reproduced from Karmakar *et al.* (2015) with permission.

which participate in the hydrogen-bonding network, leading to a 3D structure (Mao *et al.*, 1996). The use of pz and 2,3-pzdc together resulted in a coordination polymer in which pz as pillared units link sheets of Cu complexes containing tridentate 2,3-pzdc (Kondo *et al.*, 1999). In another coordination polymer of 2,3-pzdc and Cu[II] centres, the organic ligand used only three of its six possible donor sites. The N/O donor atoms of the ligand in bidentate mode occupy two equatorial positions on the square-pyramidal Cu ion with the O-donor bridgehead in the axial site forming a 1D polymeric structure. In addition to π–π interactions between two adjacent pyrazine rings, hydrogen bonding through coordinated and lattice water molecules generates the 3D structure. A study of the magnetic properties of this compound showed that there are very weak antiferromagnetic interactions between the Cu centres through the N and O atoms of the 2,3-pzdc unit, with these donor atoms in the basal and apical positions, respectively (Konar *et al.*, 2004). By changing the solvent of the reaction from water to DMSO, despite obtaining the same coordination polymer, the coordination of 2,3-pzdc to the Cu centres occurs as a tridentate ligand with one carboxylate group involved in hydrogen bonding to DMSO (Xiang *et al.*, 2004). With lead(II) halides, 2,3-pzdc forms a 1D double chain coordination polymer with the ligand coordinating in a tetradentate manner. Intra- and intermolecular hydrogen bonding to the ligand O atoms accompanied by Br^{−} bridges generates a 3D network (Fard & Morsali, 2010). The 1D coordination polymer based on the Pb$_2$Cl$_2$(2,3-Hpzdc)$_2$(H$_2$O)$_2$ monomer, when submerged in a solution containing Cu[II]

cations, undergoes cation exchange with preservation of the 1D chain without bridging halides. When solutions containing Hg[II] or Co[II] cations are used, different products are obtained. In the case of Hg[II], the [Pb$_2$(2,3-pzdc)$_4$(H$_2$O)$_2$]$^{4-}$ dimer is formed with some of the 2,3-pzdc ligands serving to construct 2D layers. It is noteworthy that the Pb—O and Pb—N bond lengths in this complex are shorter than in the starting complex. When Pb$_2$Cl$_2$(2,3-Hpzdc)$_2$(H$_2$O)$_2$ is soaked in a Co[II] solution, a structural transformation occurs and a 3D network structure based on the Pb$_3$(2,3-pzdc)$_3$(H$_2$O) unit is formed (Wardana *et al.*, 2015). Reaction of pyrazine-2,5-dicarboxylic acid (2,5-pzdc) with Zn[II] salts in dimethylformamide (DMF) solution resulted in the 1D coordination polymer [Zn(2,5-pzdc)(DMF)$_2$]$_n$ (Isaeva *et al.*, 2011).

Metal complexes of pyrazine-2,3,5,6-tetracarboxylic acid (pztc) have been studied (Ghosh & Bharadwaj, 2004, 2005, 2006; Ghosh *et al.*, 2006), with the solid-state structures being stabilized by intra- and intermolecular hydrogen bonding (Fang *et al.*, 2008). Pyrazinetetracarboxylic acid reacted with Cu[II] salts in buffer solutions containing different cations generate zigzag chains and also quasilinear polymer structures in which extensive hydrogen-bonding networks stabilized the solid-state structure (Graf *et al.*, 1993). If the above reaction is carried out with added lanthanoid ions, different frameworks result. For example, nine-coordinate Tb[III] ions are connected to each other by pztc ligands chelating through two ONO sites to generate a hexagonal assembly. On the other hand, with Eu[III] cations, the ligand coordinates in mono-, di- and tridentate modes with the inclusion of potassium ions in the solution and only one N and one O atom are left uncoordinated. An intermolecular hydrogen bond is also observed in [EuK(pztc)(H$_2$O)$_4$], whereas in [Tb$_2$(H$_2$pztc)$_3$]·3.5H$_2$O, there is an intermolecular O—H···O interaction of 2.395 (6) Å (Thuéry & Masci, 2010).

3-Carbamoylpyrazine-2-carboxylic acid (L_2) acts as a bidentate ligand in coordinating to Ni[II] ions, forming Ni(L_2)$_2$-(H$_2$O)$_2$ in which the amide moiety is uncoordinated and participates in hydrogen bonding with an adjacent molecule, generating a zigzag 1D chain. Additional hydrogen bonding expands this to the 3D structure (Heyn & Dietzel, 2007). 3-Aminopyrazine-2-carboxylate as a multidentate ligand could coordinate to transition metals (Fig. 7) and it is observed that in every case the amine groups form intramolecular N—H···O hydrogen bonds to the carboxylate group, while the
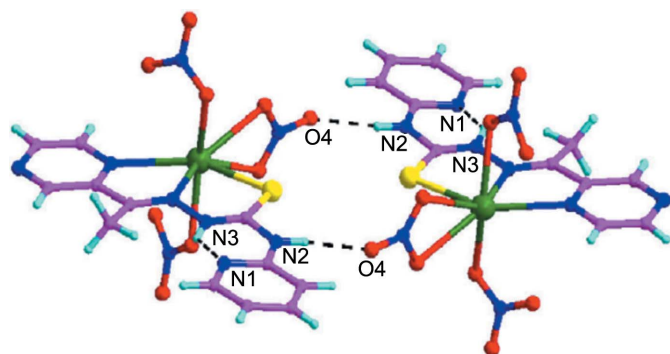

Figure 8
Hydrogen bonds (dashed lines) in [Bi(HL)(NO$_3$)$_3$]. Reproduced from Zhang, An *et al.* (2012) with permission.

remaining pyrazine N atom and the amine group participate in hydrogen-bonding interactions and construct 2D and 3D supramolecular architectures (Karmakar *et al.*, 2015; Li & Zhang, 2015; Koleša-Dobravc *et al.*, 2017; Tayebee *et al.*, 2008). It has been shown that vanadium compounds have anti-diabetic effects and complexes of vanadium with bidentate anionic organic ligands have a greater influence than vanadium inorganic moieties. In the two vanadium complexes of 3-aminopyrazine-2-carboxylic acid and 2-pyrazine-2-carboxylic acid, the central metal atom has distorted octahedral geometry, but hydrogen-bonding reinforces the structures with 3D and double-layer networks, respectively. The insulin-like activity of vanadium complexes of 3-aminopyrazine-2-carboxylic acid and pyrazine-2-carboxylic acid have been compared with $VOSO_4$ anions. It is observed that these three complexes have similar activities and a bidentate ligand, and also that an amine moiety does not effect the insulin-like activity (Koleša-Dobravc *et al.*, 2017).

2-Acetylpyrazine N^4-pyridylthiosemicarbazone (H*L*) is a compound with antimicrobial activity whose interaction with bismuth(III), a heavy metal with low toxicity, has been studied. Hence, the composition of these two segments can have different effects on the cytotoxicity. In this regard, the [Bi(H*L*)(NO₃)₃] complex, with unusual eight-coordinated Bi^{III} centres, has been reported. The results of inhibition studies of some Gram positive and Gram negative bacteria indicated that the IC_{50} values (compound concentration that produces 50% of cell death) for the complex (1.6 μ*M*) is much lower than for both the mentioned ligands (14.8 μ*M*) and Bi(NO₃)₃·5H₂O (41.6 μ*M*). Thus, its activity is comparable to that of cisplatin (1.2 μ*M*) (Fig. 8) (Zhang, An *et al.*, 2012).

N-[(*Z*)-Amino(1,4-diazin-2-yl)methylidene]-1,4-diazine-2-car-bohydrazonic acid (PZOAPZ) is a flexible molecule with two pyrazine moieties connected by a chain containing a diazine fragment, as well as amine and hydroxy functional groups. By coordinating to four metal centres, it forms polynuclear clusters (Thompson *et al.*, 2001). A 'locked' structural modification of a dinuclear complex with the tetradentate ligand was reported in which three five-membered chelate rings, and also hydrogen bonding between the coordinated water molecules and Br atoms, form a flat arrangement (Fig. 9). These interactions generate intramolecular antiferromagnetic interactions between the Cu centres through the planar O-atom linkage (Grove *et al.*, 2004).

3.1. Pyrazine-based MOF structures

Pyrazine as a two N-atom-donor ligand when coordinated to TMs can generate different sizes of multicore MOFs, such as molecular squares, larger coordination polymers, mixed-valence complexes or larger discrete assemblies (Steel & Fitchett, 2008). In the [Ag₂(pz)₃](BF₄)₂ framework, tricoordinated Ag^+ ions are first linked to the pz ligand to form a 1D zigzag chain, with additional pz linkages connecting the chains to form a 3D framework that has space for the BF_4^- anions (Carlucci *et al.*, 1995). A microwave-assisted hydrothermal synthetic technique, which reduced the reaction time, was used
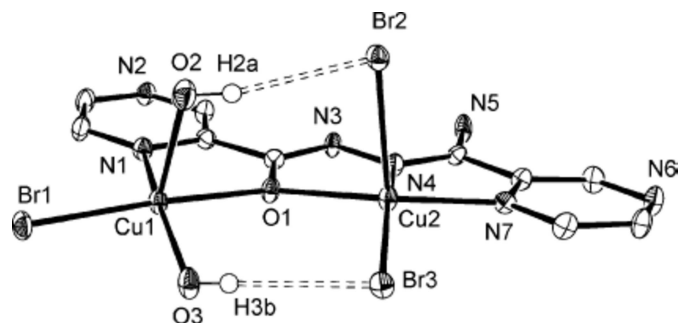

Figure 9
Structure of [Cu₂(PZOAPZ-H)Br₃(H₂O)₂]. Reproduced from Grove *et al.* (2004) with permission.

to synthesize a MOF structure based on pyrazine and copper fragments. This crystal structure consists of interpenetrating ten-membered rings with alternating pyrazine and sulfate groups linking the Cu^{II} centres. Two coordinated water molecules form short hydrogen bonds to adjacent sulfate rings to construct the 3D framework (Amo-Ochoa *et al.*, 2007). A 2D sheet MOF, *i.e.* {[Co₂(pztc)(py)₂(H₂O)₄]·4H₂O}ₙ, provides the perimeter to accommodate infinite chains of cyclic water hexamers. Among the many available donor–acceptor sites of pyrazinetetracarboxylic acid, only one carboxylate group was not involved in coordination with the Co ions. Several water molecules involved in hydrogen bonding between themselves and the uncoordinated carboxylate ion, as well as coordination to Co centres, assist in generating the overall structure (Ghosh & Bharadwaj, 2005). Bismuth-based MOFs can be attractive candidates for doping lanthanoid cations into the network due to the similarity in the ionic radii and the preferred coordination spheres of Bi^{3+} and trivalent lanthanoid ions. One example is the *in-situ* co-doping of lanthanoid ions into the 2D coordination polymer [Bi₂Cl₆(pz)₄] (Heine *et al.*, 2014). Five zinc(II) halide pyrazine coordination compounds were prepared and under ligand-poor conditions, a chain-like structure was formed, while in a ligand-rich environment, framework architectures were formed, with bidentate pz ligands occupying equatorial positions and the halides situated in axial positions (Bhosekar *et al.*, 2006).

A partnership of classical covalent and coordination bonds in the construction of MOFs is common, while bifluoride linkers, through strong F—H···F bonds can give interesting MOF structures. In the 3D {[Cu₂F(HF)(HF₂)(pz)₄][(SbF₆)₂]}ₙ framework, layers of [Cu(pz)₂]²⁺ cations are connected to each other by the HF_2^- linkages with a bond enthalpy of 175 kJ mol⁻¹. Here the hydrogen-bond strength within HF_2^- anions [H—F = 1.142 (6) Å and F—H···F = 171 (7)°] is comparable to Cu—F and Cu—N coordination bonds (Li *et al.*, 2013). In addition to the HF_2^- unit, $H_3F_4^-$ ions are observed in the solid state; these are less stable than $H_2F_3^-$ or HF_2^- segments. While $H_3F_4^-$ has the central fluoride ion hydrogen bonded to three additional HF molecules, the resulting 3D structure, *i.e.* [CuAg(H₃F₄)(pz)₅](SbF₆)₂, was similar to previously reported compounds (Manson *et al.*, 2009).

3-Aminopyrazine-2-carboxylic acid is a multicentre ligand and has the ability to establish high-dimensional structures.

Table 1
Structural and magnetic parameters of compounds with tetragonal $[Cu(pz)_2]^{2+}$ layers (T_N the Néel temperature).

Compound	Space group	Distance (Å)		Cu···Cu distance (Å)		Pz rotation angle (°)	J∥ (K)	T_N (K)
		Cu—N	Cu—X	Cu–pz–Cu	Cu–X–Cu			
$[CuCl(pz)_2]BF_4$	$P4/nbm$	2.053	2.865	6.895	5.731	58.8	9.4	3.9
$[CuBr(pz)_2]BF_4$	$P4/nbm$	2.052	2.963	6.894	5.926	55.4	8.9	3.8

This bidentate ligand can fill out the coordination spheres of metal ions and have uncoordinated fragments, such as the N atoms of pyrazine and the amine group, available for hydrogen bonding, to organize 3D frameworks with various morphologies (Tayebee *et al.*, 2008; Starosta & Leciejewicz, 2010; Cheng *et al.*, 2009; Gao & Ng, 2010; Deng *et al.*, 2010).

N-(Pyrazine-2-carbonyl)pyrazine-2-carboxamide forms complexes with di- and trivalent metals to construct 3D frameworks with a variety of structures. In the 1:2 complexes $[Co^{II}(dpzca)_2]$, $\{[Co^{III}(dpzca)_2]BF_4\}_2 \cdot 5CH_3CN$ and $[Cu^{II}(dpzca)_2]$, two tridentate dpzca ligands occupy all the coordination sites of the approximately octahedral metal ions, but the case of $[Cu^{II}(dpzca)(H_2O)_3]_2(SiF_6) \cdot 2H_2O$ is different and a large number of strong hydrogen-bonding interactions are observed. Axially coordinated water molecules are involved in hydrogen bonding in bifurcated modes with the O atoms of a neighbouring dpzca ligand to form dimers, and in further hydrogen bonding with axially coordinated water molecules from an adjacent dimer to generate double-stranded chains with water molecules and hexafluorosilicate anions (Cowan *et al.*, 2015).

4. Propagation of magnetic interactions through hydrogen bonding

Covalent bonding is generally considered as a necessary link between single-molecule magnets to facilitate interactions between them (Sessoli *et al.*, 1993; Inglis *et al.*, 2011). In this regard, pyrazine derivatives can act as a linkage between

magnetic metal centres. The role of pyrazine-2,5-dicarboxylate and pyrazine-2,3-dicarboxylate as linker groups is investigated in the spin exchange between paramagnetic metal centres. With either pyrazinedicarboxylic acid (pzdc) acting as a bis-bidentate linkage and occupying equatorial positions, the connectivity between metal centres (Mn, Fe, Zn and Cu) is observed. A low magnetic susceptibility of the copper ions is observed when a carboxylate group of the nonplanar 2,3-pzdc ligand acts as a monodentate linkage between the metals (Beobide *et al.*, 2006). Furthermore, the nature of the bridging ligand is key to the properties of the material in the solid state since it dictates the sign and magnitude of the magnetic exchange between the paramagnetic metal ions. In the 2D coordination polymer $\{[Cu_2(pztc)(py)_2(H_2O)_3] \cdot 4H_2O\}_n$, a very weak coupling between metal centres is observed, as may be expected from the pyrazinetetracarboxylate linkage with a large Cu···Cu distance (Ghosh *et al.*, 2006).

In recent years, noncovalent interactions, such as π–π stacking and hydrogen bonding, have been shown to be a new channel for magnetic exchange in supramolecular chemistry (Fukuroi *et al.*, 2014; Hicks *et al.*, 2001; Atzori *et al.*, 2014; Fitzpatrick *et al.*, 2016). $[Fe(HL)_2Cl_4]$ (L is 2-aminopyrazine) is a discrete complex having a 2D layer structure formed by halogen bonding between Cl and the N atom of the amine substituent on the pyrazine moiety of an adjacent complex. A 3D noncovalently linked assembly is generated by π–π stacking between pyrazine rings, with a distance of 3.346 (5) Å between them, and an antiferromagnetic interaction between the $S = 2$ ions was observed (Rusbridge *et al.*, 2018).

Bifluoride (HF_2^-) and fluoride (F^-) ligands in copper pyrazine complexes were observed to function as bridging and terminal units through strong hydrogen bonding to connect Cu centres with the suggestion that such compounds may work to stabilize long-range magnetic ordering at low temperature (Brown *et al.*, 2007). F···H—O hydrogen bonding (2.612 and 2.597 Å) (Fig. 10) connects the inverted 1D coordination polymer generated from the $CuF_2(H_2O)_2(pz)$ monomer into a quasi-2D lattice whose magnetic properties were studied. The magnitude of the experimental *g* factor and its reproduction through density functional theory (DFT) calculations proved that the orbitals in the CuF_2O_2 plane generate an anti-ferromagnetic square lattice. Also, a lowering of the temperature affects both the strength of the F···H—O hydrogen-bond network and the magnetic ordering (Manson *et al.*, 2008).

In further studies, the role of two types of FHF$^-$ linkages on the magnitude of the antiferromagnetic interactions was investigated. For the $[Cu(HF_2)_2(pz)]_n$ coordination polymer, one can conceive of three ways of strengthening spin
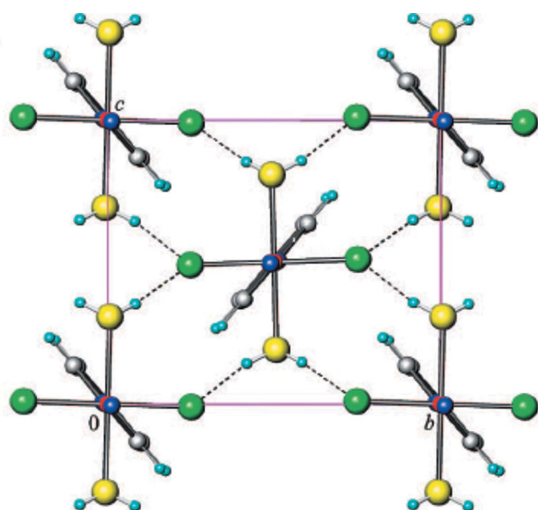

Figure 10
Chain packing arrangements of $CuF_2(H_2O)_2(pz)$, viewed along the chain axis. Dashed lines delineate O—H···F hydrogen bonds. Reproduced from Manson *et al.* (2008) with permission.

exchange. One would be through a pyrazine bridge between metal atoms, while the others would be through $\mu_{1,1}$- or $\mu_{1,3}$-bridging modes of the HF_2^- anion. The results showed that the

Cu–pz–Cu path has a weaker spin exchange, whereas a $\mu_{1,1}$-FHF$^-$, by sharing the σ-type orbitals of the F atom with the $3d$ orbitals of the Cu centre, or a $\mu_{1,3}$-mode HF_2^-, which involves
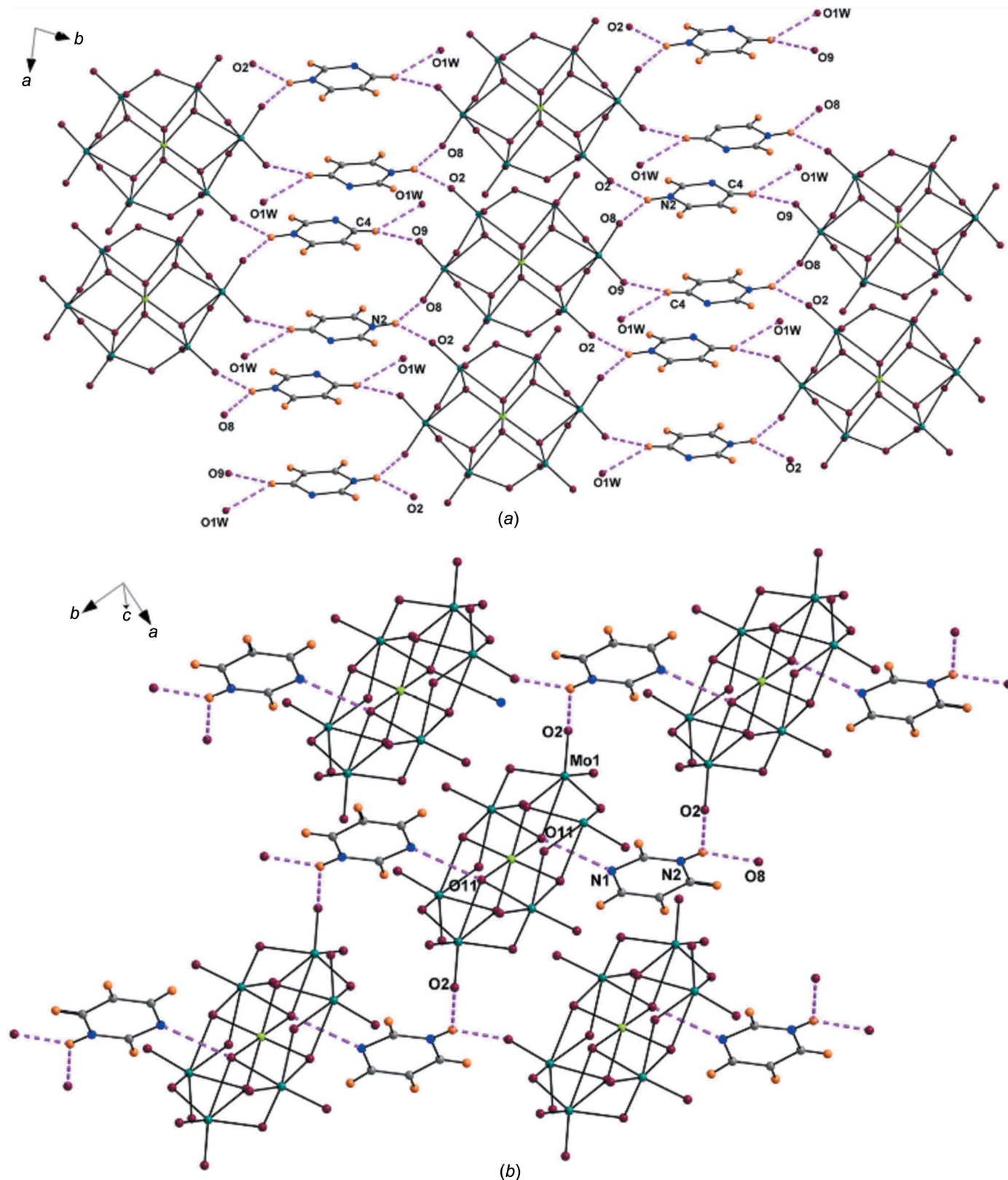

Figure 11
Representation of the (Hpym)$_2$[H$_7$CrMo$_6$O$_{24}$]·2H$_2$O sheet showing (a) N—H···O and C—H···O interactions, and (b) O—H···N interactions. Reproduced from Singh *et al.* (2014) with permission.

spin exchange through π orbitals, has a larger value (Manson, Warter *et al.*, 2011). In addition to the role of the linker in the spin exchange, the arrangement and symmetry of the linker can be of particular importance. Hence by comparison of the $[Ni(HF_2)(pz)_2]X$ ($X = PF_6^-$ and SbF_6^-) coordination polymers it was found that, in spite of similar frameworks, spin exchange through the Ni–FHF–Ni and Ni–pz–Ni pathways differed. Owing to the linear Ni–FHF–Ni linkage and also a higher crystal symmetry that leads to linear Ni–pz–Ni units in the $[Ni(HF_2)(pz)_2]SbF_6$ framework, this complex has a higher magnetic susceptibility (Manson, Lapidus *et al.*, 2011). The HF_2^- unit, as the superexchange pathway, can be actively involved in both the magnetic quantum phase transition and the series of pressure-induced structural distortions which affect the overall magnetic susceptibility (O'Neal *et al.*, 2016).

The $Cu(pz)(NO_3)_2$ and $[Cu(pz)_2(NO_3)]NO_3 \cdot H_2O$ polymers have been considered for investigation of the magnetic property of a quasi-low-dimensional quantum magnet. Although nitrate ions help to increase the dimension of the chain and lattice of $Cu(pz)_n$ through incorporating hydrogen bonding (C—H···O interactions), for the purposes of determining the feasibility of spin exchange, only the pyrazine linkage and the intermetallic distances and angles between the Cu centres have been considered (Dos Santos *et al.*, 2016).

The magnetic susceptibility of $[CuX(pz)_2]BF_4$ ($X = Cl$ or Br), with a distorted octahedral coordination of the Cu^{2+} ion by four N atoms of pyrazine and halide linkages, was investigated. It has been shown that the Cu–pz–Cu and Cu–X–Cu pathways have different values for spin exchange between Cu centres (Table 1). In spite of the shorter distance in the interlayer Cu–X–Cu interaction compared to that in the intralayer Cu–pz–Cu interaction, the molecule exhibits an elongated Jahn–Teller axis along the c axis and the unpaired electron in the $d_{x^2-y^2}$ orbital results in a quasi-2D magnetic network through σ-bonding for the Cu···N interaction (Kubus *et al.*, 2018). Consequently, complexes containing pyrazine- and halogen-based ligands, which connect magnetic metal centres through covalent and noncovalent interactions,

have an effective role in determining the magnetic susceptibility of this class of compounds.

5. Role of hydrogen bonding in the stabilization of POM-based hybrids

POMs as anionic clusters have unique properties in various fields, such as biology (Arefian *et al.*, 2017), photophysical systems (Fashapoyeh *et al.*, 2018), magnetism (Clemente-Juan *et al.*, 2012) and catalysis (Liu *et al.*, 2013). Furthermore, their electron-rich surfaces and accessible oxygen groups make them suitable candidates for the construction of two-component (type I) or three-component (type II) hybrids (Mirzaei *et al.*, 2014). Hence, incorporation of POMs into systems containing pz ligands and studies of the interactions that connect them could prove fruitful. In many POM-based hybrids, water molecules, whether coordinated to the metal atoms or simply lattice solvent molecules, can affect the dimensions of the structures (Guo *et al.*, 2016; Zhang *et al.*, 2014). It is interesting to clarify the roles of hydrogen bonds in POM-based hybrids containing pyrazine derivatives. The α-Keggin ion phosphododecamolybdate creates 3D tunnel structures for the inclusion of pyridazinium, pyrazinium and pyrimidinium ions by electrostatic interaction, while short interactions in $[(C_4H_5N_2)_3(PMo_{12}O_{40})]\cdot nH_2O$, containing N—H···O, C—H···O and O—H···O hydrogen bonds, consolidate the architecture of the crystal (Ugalde *et al.*, 1997). In further work, the four-electron reduced $[\beta\text{-}PMo_{12}O_{40}]^{3-}$ anion was reacted with the above cations, and pyridazinium was found to be incorporated by a N—H···O hydrogen bond with a ten-membered ring of hydrogen-bonded water molecules that are disposed between polyanion chains of $[\beta\text{-}PMo_{12}O_{40}]^{3-}$ subunits connected by hydrogen-bonding interactions. The pyrimidine (pym) units were hydrogen bonded to the water molecules, which formed part of a 'waterfall' along the [010] direction with the rest of the water molecules, and were also connected *via* π-interactions with the surface O atoms of the tetrameric $[\beta\text{-}PMo_{12}O_{40}]^{3-}$ units that adopt a helicoidal
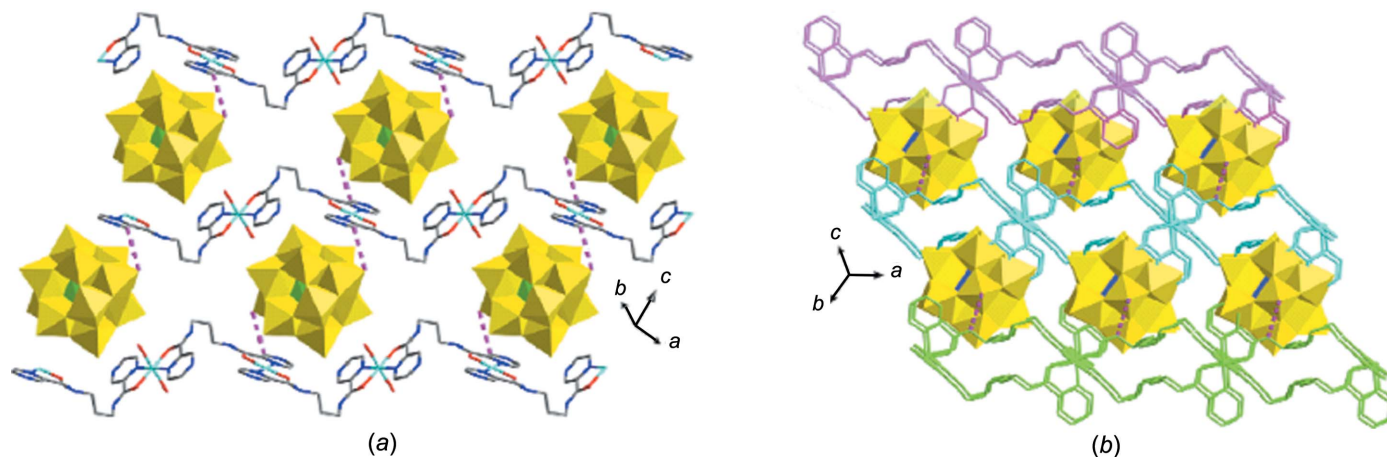

Figure 12
The 2D and 3D supramolecular structure formed *via* hydrogen bonds in (*a*) $[Cu_2(L1)_2(SiMo_{12}O_{40})(H_2O)_2]\cdot 2H_2O$ and (*b*) $[Cu_2(L2)_2(SiMo_{12}O_{40})]\cdot 2H_2O$. Reproduced from Wang *et al.* (2015) with permission.

arrangement, thereby constructing organic–inorganic hybrids. In a related study, pyrazine units, through participation of both N atoms in hydrogen bonding, create a 3D tunnel network that can accommodate the helicoidal arrangement of $[PMo_{12}O_{40}]^{3-}$ chains and construct 3D reinforced hybrids (Vitoria *et al.*, 2003). The 2-acetylpyrazinium ion also exploits $N-H\cdots O$ interactions in its interaction with $[PW_{12}O_{40}]^{3-}$ to assemble a hybrid (Liu, 2010). Interactions between the dodecylpyridazinium (C_{12}pda) cation and the decatungstate (W_{10}) anion were investigated. This cation with its long alkyl chain, unlike the pyridazinium cation itself, did not show any $\pi-\pi$ stacking or $C-H\cdots\pi$ interactions because the arrangement of the organic moieties was such that the heterocyclic portions are located away from each other. Instead, $C-H\cdots O$ hydrogen bonds between the hydrophilic head of C_{12}pda and the W_{10} anion lead to a layer structure (Otobe *et al.*, 2015).

Most of the organic/inorganic salts based on the Anderson–Evans POMs undergo 1D hydrogen-bonding interactions with strong $N-H\cdots O$ hydrogen bonding. The $(Hpym)_2[H_7Cr-Mo_6O_{24}]\cdot 2H_2O$ hybrid shows 1D $N-H\cdots O$ hydrogen-bonding interactions. Furthermore, protonated polyanions interact with uncoordinated N atoms of the cations, while water molecules participate in $C-H\cdots O$ hydrogen-bonding interactions (Fig. 11) (Singh *et al.*, 2014).

Although Anderson–Evans-type clusters link covalently to a discrete $[M(pz)_2(H_2O)_2]^{2+}$ (M = Co, Ni and Zn) complex through corner-sharing forming 1D chains, the uncoordinated N atom of pz, the protonated pyrazine and the water mol-ecules interact with the oxygen-rich surface of the {CrMo$_6$-$(OH)_6O_{18}\}^{2-}$ polyanion to firmly stabilize the structure. $[\{Ni(pz)(H_2O)_4\}_2\{CrMo_6(OH)_6O_{18}\}](CH_3COO)_2\cdot 6H_2O$ consist of linear chains of $\{Ni(pz)(H_2O)_4\}$ subunits with amplification of the 2D structure carried out by hydrogen bonding between coordinated water and the POM, and also $C-H\cdots O$ interactions with the acetate fragments (Singh *et al.*, 2010). The 3D structure of $\{[M(pz)(H_2O)_4]_2(H_3O)_2[V_{10}O_{28}]\}$ (M = Cu^{II} and Ni^{II}) is similar to many coordination polymers containing pyrazine and contains a 1D infinite chain structure, which in this case is connected to the decavanadate units by hydrogen bonding (Wang *et al.*, 2008).

Pyrazine-2-carboxylic acid has various available donor–acceptor sites so that, in addition to coordinating to metal ions, it has potential for hydrogen-bonding interactions. In the case below, pyrazine-2-carboxylic acid is used as an organic linker to form a chain-like coordination polymer. Coordinated water molecules in the Cu(2-pzc)(H$_2$O)$_2$ building blocks, in addition to joining chains by hydrogen bonding, link $[Mo_8O_{26}]^{4-}$ polyanions *via* hydrogen bonding into a coordination polymer structure (Zheng *et al.*, 2001). In another report, pyrazine-2-carboxylic acid, acting as a tridentate ligand, links Ni^{II} ions to form a 1D zigzag chain that with the $[\beta-Mo_8O_{26}]^{4-}$ anion coordinates to four Ni centres and results in an inorganic–organic hybrid compound (Li, Chen *et al.*, 2014). Pyrazine-2-carboxylic acid uses three functional groups to coordinate to Cu and Co ions, with subsequent inclusion of the Anderson–Evans cluster {CrMo$_6$(OH)$_7$O$_{17}$}, which acts as a bidentate
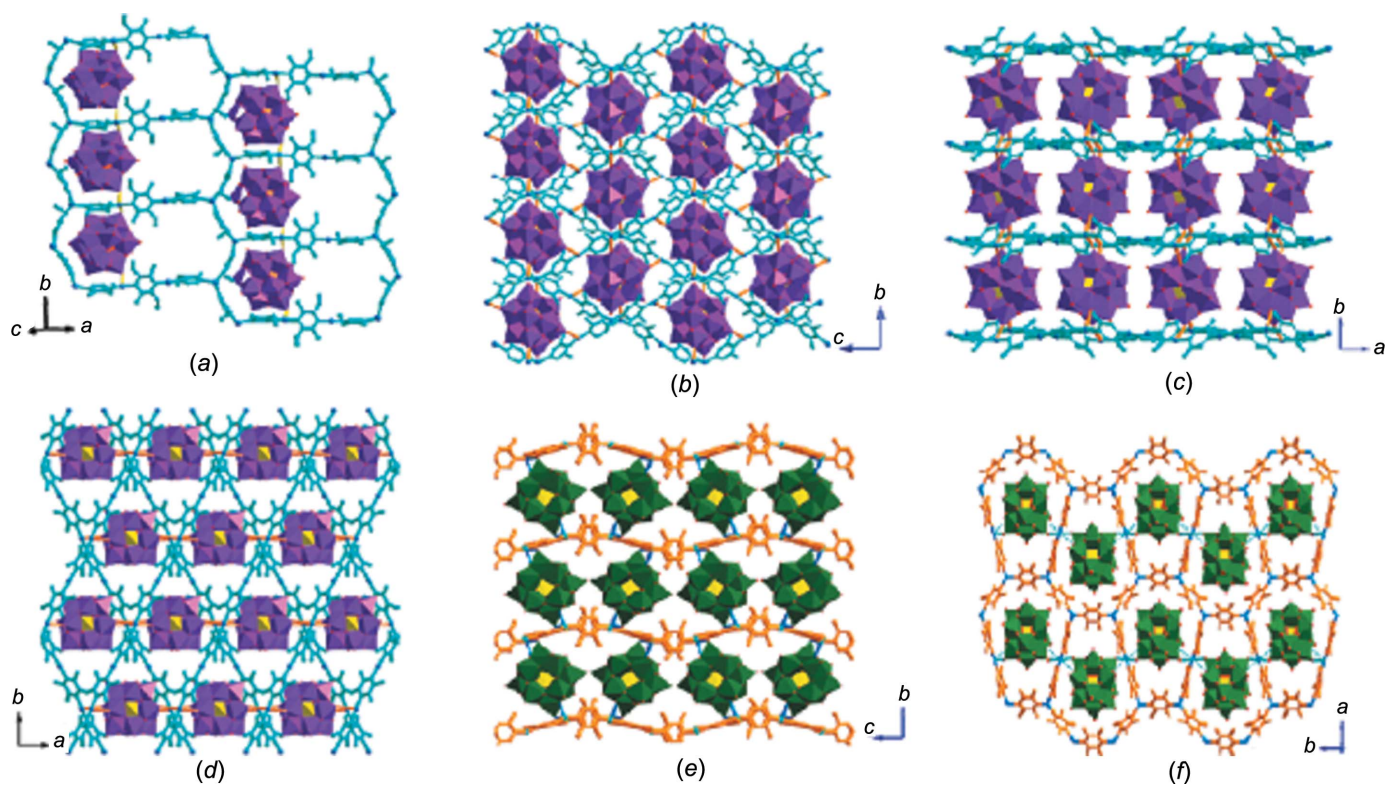

Figure 13
Perspective views of (*a*) the 3D framework in $[Cu^I_4(2Et,3Me-Pz)_5(SiW_{12}O_{40})]$, the 2D double layer in (*b*) $[Cu^I_4(2,6-Me_2Pz)_4(SiW_{12}O_{40})]$, (*c*) $[Cu^I_4(2,5-Me_2Pz)_4(SiW_{12}O_{40})(H_2O)_2]$, (*d*) $[Cu^I_4(pztc)_4(SiW_{12}O_{40})]\cdot H_2O$ and (*e*) $[Cu^I_4(2,5-Me_2Pz)_4(PMo^{VI}_{11}Mo^VO_{40})]\cdot 1.5H_2O$, and (*f*) the 2D layer in $[Cu^I_3(2,3,5-tmpz)_4(PMo_{12}O_{40})]\cdot H_2O$ (2,3,5-tmpz is 2,3,5-trimethylpyrazine). Reproduced from Liu *et al.* (2011) with permission.

inorganic linkage and forms a 1D coordination polymer. The presence of water in cavities of the ladder-like sheet, which interact with coordinated water and the POM by hydrogen bonding, forms a 3D structure from 2D layers (Singh & Ramanan, 2011). $[Na_4(H_2O)_{14}Cu(2,3-pzdc)_2]H[Al(OH)_6-Mo_6O_{18}]\cdot5H_2O$ is a rare 3D organic–inorganic compound in which the decadentate Anderson POM $[Al(OH)_6Mo_6O_{18}]^{3-}$ connects to $[Na_4(H_2O)_{14}]^{4+}$ clusters and produces 2D window-like layers. From this is generated a 3D open framework by connection to $[Cu(2,3-pzdc)_2]^{2-}$ complexes (Li et al., 2010). The configuration of POM-containing structures can depend on the type of POM used. Accordingly, two Anderson-type clusters, i.e. $[TeMo_6O_{24}]^{6-}$ and $[CrMo_6(OH)_5O_{19}]^{4-}$, are used with complexes containing 3-(pyrazin-2-yl)-5-(1H-1,2,4-triazol-3-yl)-1,2,4-triazolyl (pytty) and Co^{II} cations. The product is the first example of a 2D network consisting of a 1D Co–$TeMo_6$ inorganic chain and a 1D circle-shaped complex of the pytty ligand with adjacent inorganic cations. Finally, C—H⋯O interactions between pytty fragments and the POM formed the 3D architecture. Furthermore, C—H⋯O hydrogen bonding between the $[Co_2(H_2pytty)_2]^{4+}$ subunit and $[CrMo_6(OH)_5O_{19}]^{4-}$ anions increases the dimensions of the hybrid to a 2D network (Bai et al., 2018). In another hybrid, layers of $\{Cu_4(pztet)_5(Hpztet)(H_2O)_2\}^{3+}$ (pztet is pyrazine-tetrazole) units consist of hexa- and tetracoordinated Cu^{II} ions, while $[PMo_{12}O_{40}]^{3-}$ polyanions occupy axial positions of the Cu^{II} cations, which have an axially distorted $\{CuN_4O_2\}$ geometry, to construct a 3D POM-pillared structure (Darling et al., 2013).

A considerable number of flexible N-donor ligands have been used in POM-based metal–organic complexes (Tian et al., 2008; Meng et al., 2009; Wang et al., 2010; Zhang et al., 2011; Taleghani et al., 2016). For example, two flexible bis-pyrazine–bis-amide ligands are reacted with POM and it is seen that noncoordinated $[PMo_{12}O_{40}]^{3-}$ and $[SiMo_{12}O_{40}]^{4-}$ anions are trapped at the interface between adjacent wave-like chains of $\{[Cu(L1)]^{2+}\}_n$ [L1 is N,N′-(propane-1,3-diyl)bis(pyrazine-2-carboxamide)] cations via C—H⋯O hydrogen bonds to create a 2D supramolecular architecture (Fig. 12a). By increasing the carbon chain length, the complex forms 2D $\{[Cu(L2)]^{2+}\}_n$ [L2 = N,N′-(hexane-1,3-diyl)bis(pyrazine-2-carboxamide)] layers which connect to the $[SiMo_{12}O_{40}]^{4-}$ clusters via hydrogen bonds, thereby increasing the dimension of the supramolecular structure (Fig. 12b). When the flexible N,N′-(propane-1,3-diyl)bis(pyrazine-2-carboxamide) ligand is introduced into the reaction containing smaller POMs, interesting structures can be formed. A ribbon-like 1D chain structure, modified by incorporating tridentate $[CrMo_6(OH)_6O_{18}]^{3-}$ Anderson anions as building blocks, involves alternating POMs and Cu^{II} centres. When the POM building block is $[Mo_8O_{26}]^{4-}$, the polyanion creates a bridge between adjacent 1D helical chains to form the 2D $\{[Cu(L1)(\beta-Mo_8O_{26})_{0.5}(H_2O)_2]\cdot H_2O\}$ network (Wang et al., 2015).

In 2012, the first organic–inorganic hybrid based on rare-earth-substituted polyoxometalates (RESPs) with a polycarboxylic acid ligand was reported. Pyrazine-2,3-dicarboxylate acts as a tetradentate ligand in the $[(\alpha-SiW_{11}O_{39})RE-(H_2O)(2,3-pzdc)]^{7-}$ (RE = Y^{III}, Dy^{III}, Yb^{III} and Lu^{III}) subunit, connecting discrete RESPs and also $Cu(en)_2$ fragments (en is ethylenediamine). One uncoordinated carboxylate group participated in the hydrogen-bonding network that involved the N atoms of en and pyrazine-2,3-dicarboxylate, the surface O atoms of the POM and the coordinated and uncoordinated water molecules organized by intra- and intermolecular hydrogen bonding to form the 3D supramolecular architecture (Zhang, Zhao et al., 2012).

6. POMOFs

Numerous investigations (Rangan et al., 2000; Yaghi & Li, 1996; Hennigar et al., 1997; Noro et al., 2000; Tong & Chen, 2000) proved that the nature of the MOFs depends on several
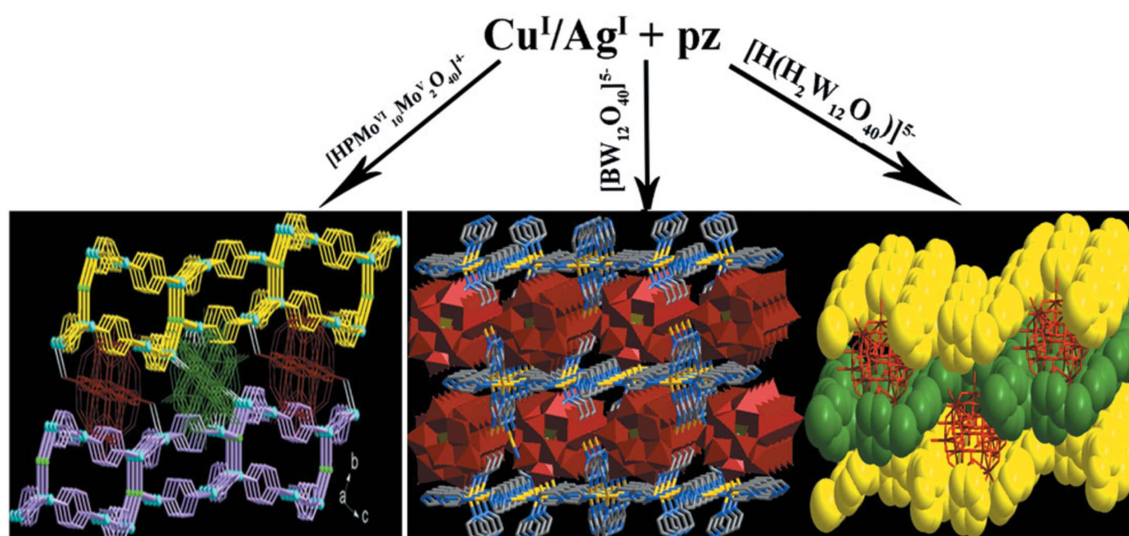

Figure 14
Summary of the formation of three porous coordination polymers templated by different Keggin ions. Reproduced from Zhu et al. (2011b) with permission.

factors, such as the type and oxidation state of the metal ion, the steric hindrance of the ligand, the metal-to-ligand ratio and the appropriate template guest molecules. POM clusters usually serve in one of three roles, namely pillar, template and node in POMOFs. Design strategies for the construction of 3D POMOFs recognize some problems: (i) POMs have surface O atoms which provide abundant potential coordination sites to link the transition-metal ions, but the low electron density and large steric hindrance cause them to rarely generate POMOFs; (ii) the size of the MOF is not large enough and it is hard to accommodate the cluster. Furthermore, the selection of the organic ligand which is to be part of the framework organization needs to be effective. Pyrazine ligands may be useful here because of their multiple sites for coordination and hydrogen bonding (Cong *et al.*, 2018). Therefore, in this section, we examine interactions that bind POMs in the voids of MOFs, either covalently or not, and the effects of the pyrazine-based ligand and the metal centre in these interactions.

6.1. POMOF-based covalent interactions

Bowl-like complexes of pz and Cu^I cations were prepared that act as hosts for the $[PMo_{12}O_{40}]^{3-}$ guest in which the Cu—O distance is 2.865 Å (Zhang *et al.*, 2009). $(H_4pzdc)_5$-$[(H_2pzdc)_6(pzdc)_2(H_2O)_2Na_6][PW_{12}O_{40}]_4 \cdot 31H_2O$ is the first example of a host–guest compound with double-Keggin anions acting as the coordinating template. They are incorporated in a double bowl-like structure $[Na_6(H_2pzdc)_6$-$(pzdc)_2]^{2+}$ by ionic Na—O and Na—N bonds. Inclusion of the $[PW_{12}O_{40}]^{3-}$ template along the [201] direction produced a 2D hybrid architecture. This 2D host–guest framework filled the interlayer spaces *via* extensive hydrogen-bonding interactions with free H_2pzdc fragments and water molecules, and stabilized the structure (An *et al.*, 2010). In the $[Cu(pz)]_3[PW_{12}O_{40}]$ organic–inorganic hybrid, pyrazine and Cu cations form 1D

chains that combine with the 1D inorganic chain generated from Cu cations and O atoms of the POM to form a 3D framework (Yang *et al.*, 2014). In a complex with Ag^+ ions and pz ligands paired with $[SiW_{12}O_{40}]^{4-}$ anions, two decanuclear rings linked by pz ligands are formed and tetradentate $[SiW_{12}O_{40}]^{4-}$ anions are coordinated to four Ag^+ ions, leading to a twofold interpenetrating structure (Zhou *et al.*, 2014).

Other POMOFs which have been reported include one with 2-ethyl-3-methylpyrazine (2Et,3Me-Pz) ligands linking Cu^I ions to generate a 2D (10,3) sheet with a hexagonal window having dimensions $19.691 \times 6.659 \times 6.659$ Å. The inclusion of $[SiW_{12}O_{40}]^{4-}$ anions in four-connected linkages surrounded by four Cu–2Et,3Me-Pz chains leads to a 3D framework structure (Fig. 13a). In another compound, the 2,6-dimethylpyrazine $(2,6-Me_2pz)$ ligand and Cu^I cations form a 1D zigzag chain which couples with hexadentate $[SiW_{12}O_{40}]^{4-}$ anions and other Cu atoms to yield a 3D structure (Fig. 13b). Neighbouring 1D chains of the 2,5-dimethylpyrazine–Cu (2,5-Me_2pz–Cu) units are connected to tetradentate $[SiW_{12}O_{40}]^{4-}$ POM anions and generate a $(4^2.6^4)(4^1.6^4.8^1)$ topology (Fig. 13c). When the 2,3,5,6-tetramethylpyrazine (2,3,5,6-Me_4pz) ligand is used in this system, a similar topology results, but the coordination environments of the cations and their packing mode are different (Fig. 13d). Changing the POM to $[PMo_{12}O_{40}]^{3-}$ units, but keeping the rest the same as above, led to changes in the coordination mode and differences in the final structures (Figs. 13e and 13f) (Liu *et al.*, 2011).

In the $[Cu_5(pz)_6Cl(SiW_{12}O_{40})]$ hybrid, a 2D sheet with 6^3 topology is formed, with the Keggin units sandwiched between the layers; Cl bridges generate the final 3D structure (Li *et al.*, 2018). However, in $[Ag_4(pz)_3(H_2O)_2(SiW_{12}O_{40})]$, the Ag^I ions create a 2D layer involving one N atom of pyrazine, two O atoms from two different $[SiW_{12}O_{40}]^{4-}$ anions and one water molecule. The Ag(pz) chain is then connected to the Keggin POMs to make the overall 3D framework (Cui *et al.*, 2010). When POM templates are reacted with Cu^I/Ag–pz coordina-
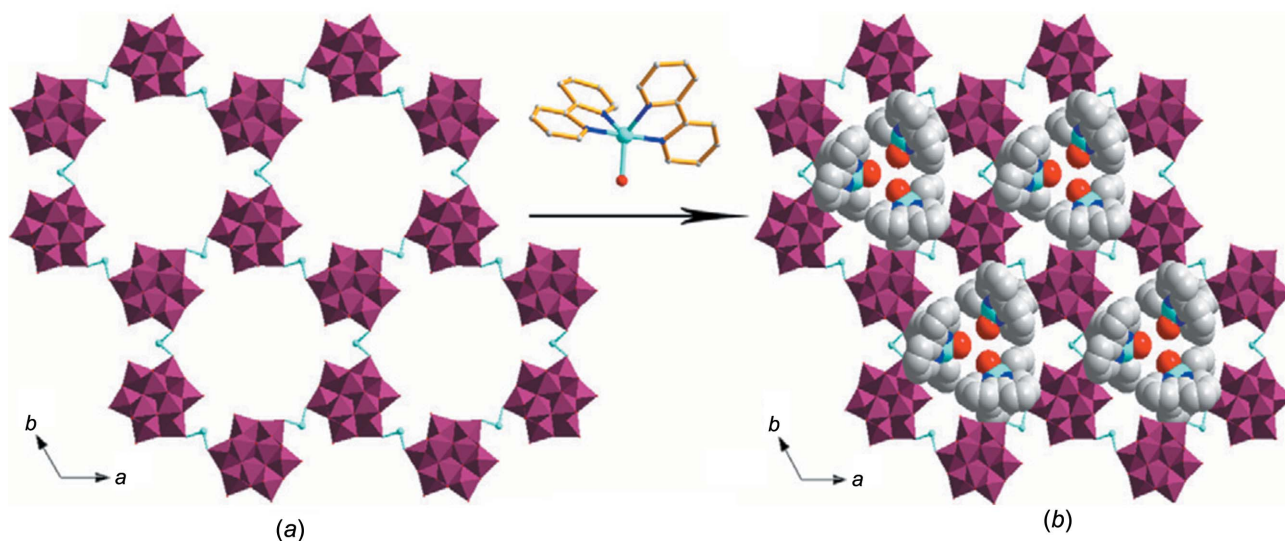

Figure 15
Views of (a) the inorganic P_2W_{18}–Cu layer with large circular voids and (b) the $[Cu^{II}(2,2'-bipy)_2(H_2O)]^{2+}$ counter-cations filling the voids. Reproduced from Zhu *et al.* (2011a) with permission.

feature articles

tion polymers, [Cu(pz)$_6$Cl][HPMoMoO$_{40}$] is produced. The structure consists of two double-layer coordination compounds with hexagonal and decagonal voids connected to each other by Cl bridges. Inclusion of two types of [PMo$_{12}$O$_{40}$]$^{3-}$ anions, that act as bidentate and hexadentate units, construct a 3D POM framework. The [Cu$_3$(pz)$_3$Cl][Cu$_2$-(pz)$_3$(H$_2$O)][PMo$_{12}$O$_{40}$] organic–inorganic hybrid has a similar framework to the previous hybrid but differs in some details (Qi *et al.*, 2013). The Ag–pz coordination framework constructs parallelogram-like voids that incorporate [BW$_{12}$O$_{40}$]$^{5-}$ POMs with eight Ag—O coordination bonds. Use of the [H$_2$W$_{12}$O$_{40}$]$^{6-}$ polyanion between 12-node layers of Cu^I–pz subunits through weak Cu$\cdots$O interactions gave a 3D POM-based inorganic–organic hybrid (Fig. 14) (Zhu *et al.*, 2011b).

Crystal structures of high-dimensional POMOFs containing monosubstituted Keggin anion chains have been reported less frequently; however, [Cu$^{II}_4$Cu$^I_2$(pzc)$_6$(HPCuMo$_{11}$O$_{39}$)-(H$_2$O)$_6$]·2H$_2$O is the first example of a 3D POMOF constructed from monosubstituted Keggin anions and N-heterocyclic carboxylate ligands. The 1D inorganic Keggin chain that is formed by sharing terminal O atoms interacts with the 1D metal–organic {[Cu$_6$(2-pzc)$_6$]$^{4+}$}$_n$ chain in which pyrazine-2-carboxylic acid acts as a di- and a tridentate ligand coordinated to Cu^I/Cu^{II} cations (Wang *et al.*, 2014).

When pz and 2,2′-bipyridine (2,2′-bipy) mixed ligands were used to construct Wells–Dawson POM-based compounds, Cu^I–pz chains and porous P$_2$W$_{18}$–Cu layers are crosslinked over Cu atoms and construct a 3D framework with a (6^3)(6^{2}8^4) topology. The [Cu^{II}(2,2′-bipy)$_2$(H$_2$O)] complex has multiple roles and not only acts as a charge-balance segment, but also as a template in the inorganic pores (Fig. 15) (Zhu *et al.*, 2011a).

6.2. POMOF-based noncovalent interactions

Some POMOFs based on pyrazine- and methylpyrazine-derived complexes have been reported in which POMs are grafted into 2D voids with noncovalent interactions. In the presence of pyrazine or 2,3-dimethylpyrazine (2,3-Me$_2$pz) ligands and Cu^{II} cations, the frameworks formed have a 4^{1}8^2 topology. These three POMOFs, {[Cu(2,3-Me$_2$pz)(2,5-Me$_2$-pz)$_{0.5}$]$_4$(SiW$_{12}$O$_{40}$)(2,5-Me$_2$pz)}$_n$, {[Cu(2-Mepz)$_{1.5}$]$_3$(PMo$_{12}$-O$_{40}$)(H$_2$O)$_{3.5}$}$_n$ and {[Ag(2,3-Me$_2$pz)$_{1.5}$]$_4$(SiW$_{12}$O$_{40}$)}$_n$, have the same 6^3 network. Although it is considered that electrostatic interactions hold the structure together, one cannot disregard hydrogen-bond interactions between methyl H atoms and the aromatic ring with O atoms on the POM surface. In this manner, H$_2$O molecules can also take part in the stabilization of these structures. Two H$_2$O units in {[Cu(pz)$_{1.5}$]$_4$(Si-W$_{12}$O$_{40}$)·2H$_2$O}$_n$ coordinated to the Cu^I ion are connected to two [SiW$_{12}$O$_{40}$]$^{4-}$ subunits by hydrogen bonding (Kong *et al.*, 2006). In the reaction of the [PW$_{12}$O$_{40}$]$^{3-}$ polyanion with the Cu^{II} ion and pz ligand, a Cu$_{12}$(pz)$_{12}$ loop-based coordination polymer templated by double-Keggin anions was obtained. A staggered packing of 2D layers leads to a sandwich-type template and decreases the intermolecular repulsions. Furthermore, C—H$\cdots$O hydrogen-bonding interactions between the pyrazine ligands and [PW$_{12}$O$_{40}$]$^{3-}$ subunits stabilize the hybrid (Li, Ma *et al.*, 2014). Two different Cu^I/pz frameworks were reported to construct a 3D organic–inorganic hybrid on reaction with [PMo$_{12}$O$_{40}$]$^{3-}$ anions. Cu(pz) chains crossed over each other and created cubic-like chambers with dimensions 13.038 × 13.038 × 13.038 Å and, with insertion of [PMo$_{12}$O$_{40}$]$^{3-}$ guest anions, formed two types of void (Fig. 16a). In the other framework, with a 2D 4^{1}8^2 network, one observes octagonal and square voids with

Figure 16
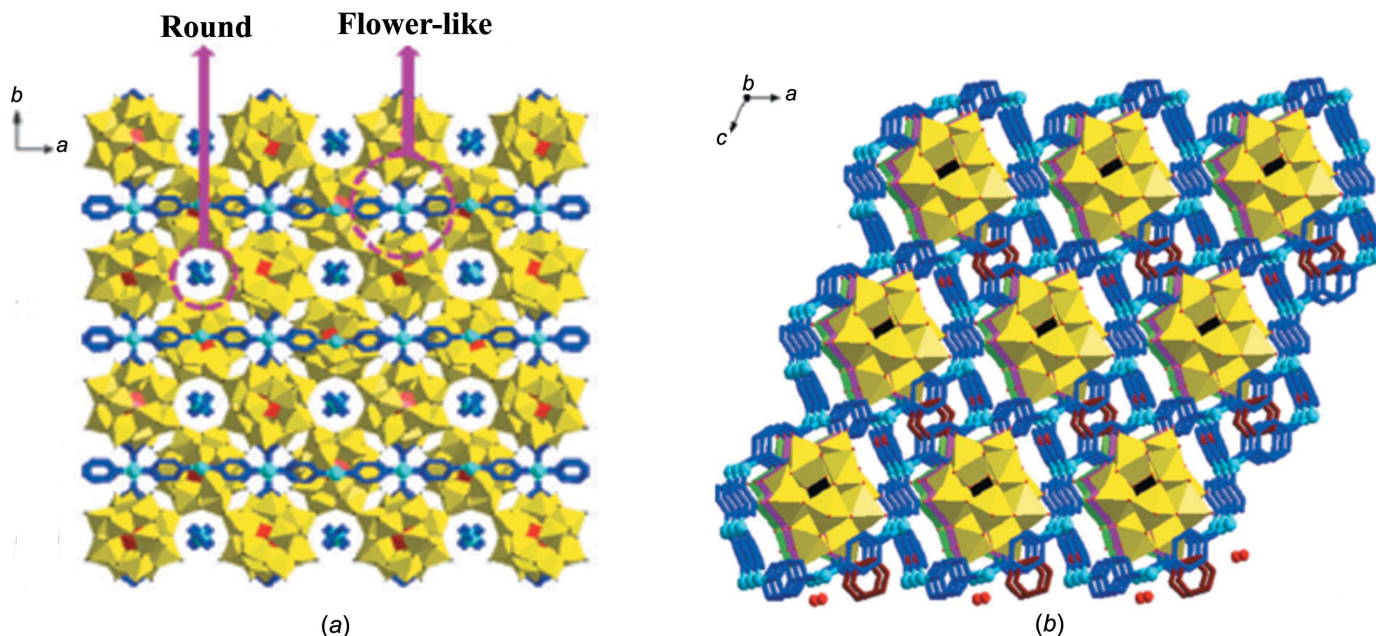Stick/polyhedral view of the 3D structure of (*a*) [Cu^I(pz)]$_3$[PMo$^{VI}_{12}$O$_{40}$] and (*b*) [Cu^I(pz)$_{1.5}$]$_4$[PMo^{V}Mo$^{VI}_{11}$O$_{40}$]·pz·2H$_2$O, along the crystallographic *b* axis. Reproduced from Qi *et al.* (2013) with permission.

dimensions 14.087 × 17.497 Å and 6.826 × 6.929 Å, respectively, with the $[PMo_{12}O_{40}]^{3-}$ clusters occupying the larger void (Fig. 16b). Again, hydrogen bonding, such as C—H···O interactions, that surround the $[PMo_{12}O_{40}]^{3-}$ units need to be considered (Qi et al., 2013).

Most recently, the 3D POMOF $[\{C_{14}Cu_{10}(pz)_{11}\}\{As_2W_{18}O_{62}\}]\cdot1.5H_2O$, with a $\{3.4.5^6.6^7\}^2\{3.4^6.5^3\}^2\{3^2.4^2.5^6.6^5\}$ topology, was reported. The 3D $\{C_{14}Cu_{10}(pz)_{11}\}$ complexes, via coordination of the Cu centre with the N atoms of pyrazine units and chloride bridges, establish two channels which provide void space for the accommodation of classical Wells–Dawson $[As_2W_{18}O_{62}]^{6-}$ clusters. The eight coordination sites of the surface O atoms of the $[As_2W_{18}O_{62}]^{6-}$ POM are used for connection with Cu ions, while the H atoms of pyrazine are involved in C—H···O hydrogen-bonding interactions which help to stabilize the structure (Cong et al., 2018).

$[Mo_8O_{26}]^{4-}$ and $[V_{10}O_{28}H_4]^{2-}$ anions are included in the coordination polymer containing pyrazine-2-carboxylic acid and a copper cation. Besides the anions producing 1D zigzag chain-like structures and 2D sheets, respectively, intermolecular interactions between fragments reinforce the final structure. Extensive hydrogen bonding is observed in susceptible sites containing O atoms of the carboxylate and coordinated and lattice water molecules and also oxygen-rich surfaces of the polyanions leading to fortified polymers. However, in the absence of the isopolyanions, only the mononuclear compound $Cu(2-pzc)_2(H_2O)_2$ was formed (Zheng et al., 2001).

Phenazine (phnz) is a ligand with a short length and it is expected that its MOFs would have small pores. Hence, two types of Lindqvist polyanion are utilized in the $[Cu_2(phnz)_3]$ coordination polymers and it was shown that these POMs $[M_6O_{19}]$ (M = Mo or W) could be placed in the 2D honeycomb voids with 6^3 topology and also through C—H···O hydrogen-bonding interactions with adjacent sheets to form a 3D coordination polymer (Sha et al., 2009). The effect of changes in the organic ligand in POM-based hybrids was investigated. In the presence of phenazine, which acts as a mono- and bidentate bridging ligand, the discrete $[Ag_4(phnz)_6(SiW_{12}O_{40})]$ cluster was formed, whereas hydrogen bonding (C—H···O interaction between the phnz and POM fragments) and π–π stacking formed the 3D supramolecular structure. By using pyrazine, which has a smaller steric hindrance, the structure will be different and three types of Ag^I segments are present. There is firstly the wave-like chain consisting of covalently-linked $[Ag_2(phnz)(pz)(H_2O)]^{2+}$ cations with $[SiW_{12}O_{40}]^{4-}$ anions and secondly the 'S'-like chain formed by hydrogen-bonding interactions between the $[Ag(phnz)(pz)]^+$ cation and the $[SiW_{12}O_{40}]^{4-}$ anion. These two types of chains act together to construct a sheet structure. Finally, the remaining fragment, $[Ag_2(phnz)_3]^{2+}$, is connected to the POM via hydrogen bonding and leads to the final hybrid (Zhu et al., 2010).

7. Conclusion

This review highlights different aspects of the pyrazine ligand and its derivatives for the construction of metal complexes having multinuclear structures. The available donor–acceptor sites of these ligands make them capable of forming intra- and intermolecular hydrogen bonds which can help to increase the dimension of the structures involved in the construction of coordination polymers and especially MOFs. It was interesting that the pyrazine ligand can have a spin-exchange role for inducing magnetic exchange through σ-bonds, particularly in the presence of H-atom-donor groups, such as HF_2^-, whose hydrogen-bonding interactions strengthen spin exchange. Pyrazine ligands can act as bridges to form pillared MOF structures with various pore sizes. Other studies on metal–pyrazine complexes containing POMs in their frameworks demonstrate the role of hydrogen bonding in these supramolecular architectures.

References

Amo-Ochoa, P., Givaja, G., Miguel, P. J. S., Castillo, O. & Zamora, F. (2007). *Inorg. Chem. Commun.* **10**, 921–924.

An, H., Xu, T., Zheng, H. & Han, Z. (2010). *Inorg. Chem. Commun.* **13**, 302–305.

Arefian, M., Mirzaei, M., Eshtiagh-Hosseini, H. & Frontera, A. (2017). *Dalton Trans.* **46**, 6812–6829.

Atzori, M., Artizzu, F., Sessini, E., Marchiò, L., Loche, D., Serpe, A., Deplano, P., Concas, G., Pop, F., Avarvari, N. & Laura Mercuri, M. (2014). *Dalton Trans.* **43**, 7006–7019.

Aubert, E., Mamane, V. & Fort, Y. (2007). *Acta Cryst.* E**63**, o4306–o4307.

Babu, N. J. & Nangia, A. (2006). *Cryst. Growth Des.* **6**, 1995–1999.

Babu, N. J. & Nangia, A. (2007). *CrystEngComm*, **9**, 980–983.

Baddeley, T. C., Howie, R. A., da Silva Lima, C. H., Kaiser, C. R., de Souza, M. V., Wardell, J. L. & Wardell, S. M. (2009). *Z. Kristallogr. Cryst. Mater.* **224**, 506–514.

Bai, S., Liu, X., Zhu, K., Wu, S. & Zhou, H. (2016). *Nat. Energ.* **1**, 16094.

Bai, X., Lin, H., Sun, J., Liu, G., Wang, X. & Wang, X. (2018). *Inorg. Chem. Commun.* **92**, 151–156.

Beobide, G., Castillo, O., Luque, A., García-Couceiro, U., García-Terán, J. P. & Román, P. (2006). *Inorg. Chem.* **45**, 5367–5382.

Bernstein, J., Davis, R. E., Shimoni, L. & Chang, N. L. (1995). *Angew. Chem. Int. Ed. Engl.* **34**, 1555–1573.

Berrah, F., Bouacida, S. & Roisnel, T. (2011). *Acta Cryst.* E**67**, o1409–o1410.

Bhosekar, G., Jess, I. & Näther, C. (2006). *Inorg. Chem.* **45**, 6508–6515.

Brown, S., Cao, J., Musfeldt, J., Conner, M., McConnell, A., Southerland, H., Manson, J., Schlueter, J., Phillips, M., Turnbull, M. & Landee, C. P. (2007). *Inorg. Chem.* **46**, 8577–8583.

Carlucci, L., Ciani, G., Proserpio, D. M. & Sironi, A. (1995). *J. Am. Chem. Soc.* **117**, 4562–4569.

Cheng, W., Shen, F.-C., Xue, Y., Luo, X., Fang, M., Lan, Y. & Xu, Y. (2018). *ACS Appl. Energ. Mater.* **1**, 4931–4938.

Cheng, X.-L., Gao, S. & Ng, S. W. (2009). *Acta Cryst.* E**65**, m1631–m1632.

feature articles

Clemente-Juan, J. M., Coronado, E. & Gaita-Ariño, A. (2012). *Chem. Soc. Rev.* **41**, 7464–7478.

Cockroft, S. L. & Hunter, C. A. (2007). *Chem. Soc. Rev.* **36**, 172–188.

Cong, B.-W., Su, Z.-H., Zhao, Z.-F., Zhao, W.-Q., Ma, X.-J., Xu, Q. & Du, L.-J. (2018). *New J. Chem.* **42**, 4596–4602.

Cowan, M. G., Miller, R. G. & Brooker, S. (2015). *Dalton Trans.* **44**, 2880–2892.

Cui, F.-Y., Ma, X.-Y., Li, C., Dong, T., Gao, Y.-Z., Han, Z.-G., Chi, Y.-N. & Hu, C.-W. (2010). *J. Solid State Chem.* **183**, 2925–2931.

Darling, K., Smith, T. M., Vargas, J., O'Connor, C. J. & Zubieta, J. (2013). *Inorg. Chem. Commun.* **32**, 1–4.

Deng, Z.-P., Kang, W., Huo, L.-H., Zhao, H. & Gao, S. (2010). *Dalton Trans.* **39**, 6276–6284.

Dos Santos, L. H., Lanza, A., Barton, A. M., Brambleby, J., Blackmore, W. J., Goddard, P. A., Xiao, F., Williams, R. C., Lancaster, T., Pratt, F. L., Blundell, S. J., Singleton, J., Manson, J. L. & Macchi, P. (2016). *J. Am. Chem. Soc.* **138**, 2280–2291.

Etter, M. C. (1990). *Acc. Chem. Res.* **23**, 120–126.

Fang, S.-R., Yang, A.-H., Zhang, Y.-P., Gao, H.-L. & Cui, J.-Z. (2008). *J. Chem. Crystallogr.* **38**, 393–396.

Fard, M. J. S. & Morsali, A. (2010). *J. Inorg. Organomet. Polym.* **20**, 727–732.

Fashapoyeh, M. A., Mirzaei, M., Eshtiagh-Hosseini, H., Rajagopal, A., Lechner, M., Liu, R. & Streb, C. (2018). *ChemComm*, **54**, 10427–10430.

Fitzpatrick, A., Stepanovic, S., Müller-Bunz, H., Gruden-Pavlović, M., García-Fernández, P. & Morgan, G. (2016). *Dalton Trans.* **45**, 6702–6708.

Fukuroi, K., Takahashi, K., Mochida, T., Sakurai, T., Ohta, H., Yamamoto, T., Einaga, Y. & Mori, H. (2014). *Angew. Chem.* **126**, 2014–2017.

Gao, S. & Ng, S. W. (2010). *Acta Cryst.* E**66**, m1466.

Ghosh, S. K. & Bharadwaj, P. K. (2004). *Inorg. Chem.* **43**, 6887–6889.

Ghosh, S. K. & Bharadwaj, P. K. (2005). *Eur. J. Inorg. Chem.* pp. 4880–4885.

Ghosh, S. K. & Bharadwaj, P. K. (2006). *J. Mol. Struct.* **796**, 119–122.

Ghosh, S. K., El Fallah, M. S., Ribas, J. & Bharadwaj, P. K. (2006). *Inorg. Chim. Acta*, **359**, 468–474.

Gilardi, R. D. & Butcher, R. J. (2001*a*). *Acta Cryst.* E**57**, o738–o740.

Gilardi, R. D. & Butcher, R. J. (2001*b*). *Acta Cryst.* E**57**, o757–o759.

Giménez-Marqués, M., Hidalgo, T., Serre, C. & Horcajada, P. (2016). *Coord. Chem. Rev.* **307**, 342–360.

Gomes, L. R., Low, J. N., Rodrigues, A. S. M. C., Wardell, J. L., Lima, C. H. da S. & de Souza, M. V. N. (2013). *Acta Cryst.* C**69**, 549–555.

Graf, M., Stoeckli-Evans, H., Whitaker, C., Marioni, I. P. P.-A. & Marty, W. (1993). *Chimia*, **47**, 202–205.

Grove, H., Kelly, T. L., Thompson, L. K., Zhao, L., Xu, Z., Abedin, T. S., Miller, D. O., Goeta, A. E., Wilson, C. & Howard, J. A. (2004). *Inorg. Chem.* **43**, 4278–4288.

Guo, L.-Y., Zeng, S.-Y., Jagličić, Z., Hu, Q.-D., Wang, S.-X., Wang, Z. & Sun, D. (2016). *Inorg. Chem.* **55**, 9006–9011.

Heine, J., Wehner, T., Bertermann, R., Steffen, A. & Müller-Buschbaum, K. (2014). *Inorg. Chem.* **53**, 7197–7203.

Hennigar, T. L., MacQuarrie, D. C., Losier, P., Rogers, R. D. & Zaworotko, M. J. (1997). *Angew. Chem. Int. Ed. Engl.* **36**, 972–973.

Heyn, R. H. & Dietzel, P. D. C. (2007). *J. Coord. Chem.* **60**, 431–437.

Hicks, R. G., Lemaire, M. T., Öhrström, L., Richardson, J. F., Thompson, L. K. & Xu, Z. (2001). *J. Am. Chem. Soc.* **123**, 7154–7159.

Huang, Y.-B., Liang, J., Wang, X.-S. & Cao, R. (2017). *Chem. Soc. Rev.* **46**, 126–157.

Inglis, R., Houton, E., Liu, J., Prescimone, A., Cano, J., Piligkos, S., Hill, S., Jones, L. F. & Brechin, E. K. (2011). *Dalton Trans.* **40**, 9999–10006.

Isaeva, V., Chernyshev, V., Afonina, E., Tkachenko, O., Klementiev, K., Nissenbaum, V., Grünert, W. & Kustov, L. (2011). *Inorg. Chim. Acta*, **376**, 367–372.

Karmakar, A., Hazra, S., Guedes da Silva, M. F. C. & Pombeiro, A. J. (2015). *Dalton Trans.* **44**, 268–280.

Khavasi, H. R., Hosseini, M., Tehrani, A. A. & Naderi, S. (2014). *CrystEngComm*, **16**, 4546–4553.

Khavasi, H. R. & Tehrani, A. A. (2013). *CrystEngComm*, **15**, 5813–5820.

Koleša-Dobravc, T., Maejima, K., Yoshikawa, Y., Meden, A., Yasui, H. & Perdih, F. (2017). *New J. Chem.* **41**, 735–746.

Konar, S., Manna, S. C., Zangrando, E. & Chaudhuri, N. R. (2004). *Inorg. Chim. Acta*, **357**, 1593–1597.

Kondo, M., Okubo, T., Asami, A., Noro, S., Yoshitomi, T., Kitagawa, S., Ishii, T., Matsuzaka, H. & Seki, K. (1999). *Angew. Chem. Int. Ed.* **38**, 140–143.

Kong, X.-J., Ren, Y.-P., Zheng, P.-Q., Long, Y.-X., Long, L.-S., Huang, R.-B. & Zheng, L.-S. (2006). *Inorg. Chem.* **45**, 10702–10711.

Kubus, M., Lanza, A., Scatena, R., Dos Santos, L. H., Wehinger, B., Casati, N., Fiolka, C., Keller, L., Macchi, P., Rüegg, C. & Krämer, K. W. (2018). *Inorg. Chem.* **57**, 4934–4943.

Kumazawa, K., Biradha, K., Kusukawa, T., Okano, T. & Fujita, M. (2003). *Angew. Chem. Int. Ed.* **42**, 3909–3913.

Li, G.-S. & Zhang, H.-L. (2015). *J. Struct. Chem.* **56**, 1613–1618.

Li, S., Ma, H., Pang, H., Zhang, L. & Zhang, Z. (2014). *New J. Chem.* **38**, 4963–4969.

Li, S., Ma, P., Wang, J., Guo, Y., Niu, H., Zhao, J. & Niu, J. (2010). *CrystEngComm*, **12**, 1718–1721.

Li, W., Kiran, M., Manson, J. L., Schlueter, J. A., Thirumurugan, A., Ramamurty, U. & Cheetham, A. K. (2013). *ChemComm*, **49**, 4471–4473.

Li, X., Li, S., Wang, Y., Zhou, K., Li, P. & Sha, J. (2018). *Polyhedron*, **151**, 206–212.

Li, X.-M., Chen, Y.-G., Zhou, S. & Shi, T. (2014). *J. Cluster Sci.* **25**, 1687–1693.

Liu, H.-X. (2010). *Z. Kristallogr. New Cryst. Struct.* **225**, 243–244.

Liu, H.-Y., Wu, H., Yang, J., Liu, Y.-Y., Ma, J.-F. & Bai, H.-Y. (2011). *Cryst. Growth Des.* **11**, 1786–1797.

Liu, X., Wang, L., Yin, X. & Huang, R. (2013). *Eur. J. Inorg. Chem.* pp. 2181–2187.

Manson, J. L., Conner, M. M., Schlueter, J. A. & Hyzer, K. A. (2007). *Polyhedron*, **26**, 1912–1916.

Manson, J. L., Conner, M. M., Schlueter, J. A., McConnell, A. C., Southerland, H. I., Malfant, I., Lancaster, T., Blundell, S. J., Brooks, M. L., Pratt, F. L., Singleton, J., McDonald, R. D., Lee, C. & Whangbo, M. (2008). *Chem. Mater.* **20**, 7408–7416.

Manson, J. L., Lapidus, S. H., Stephens, P. W., Peterson, P. K., Carreiro, K. E., Southerland, H. I., Lancaster, T., Blundell, S. J., Steele, A. J., Goddard, P. A., Pratt, F. L., Singleton, J., Kohama, Y., McDonald, R. D., Del Sesto, R. E., Smith, N. A., Bendix, J., Zvyagin, S. A., Kang, J., Lee, C., Whangbo, M. H., Zapf, V. S. & Plonczak, A. (2011). *Inorg. Chem.* **50**, 5990–6009.

Manson, J. L., Schlueter, J. A., Funk, K. A., Southerland, H. I., Twamley, B., Lancaster, T., Blundell, S. J., Baker, P. J., Pratt, F. L., Singleton, J., McDonald, R. D., Goddard, P. A., Sengupta, P., Batista, C. D., Ding, L., Lee, C., Whangbo, M. H., Franke, I., Cox, S., Baines, C. & Trial, D. (2009). *J. Am. Chem. Soc.* **131**, 6733–6747.

Manson, J. L., Warter, M. L., Schlueter, J. A., Lancaster, T., Steele, A. J., Blundell, S. J., Pratt, F. L., Singleton, J., McDonald, R. D., Lee, C., Whangbo, M. & Plonczak, A. (2011). *Angew. Chem. Int. Ed.* **50**, 1573–1576.

Manson, J. L. C. M. M., Schlueter, J. A., Lancaster, T., Blundell, S. J., Brooks, M. L., Pratt, F. L., Papageorgiou, T., Bianchi, A. D., Wosnitzae, J. & Whangbo, M.-H. (2006). *ChemComm*, **9**, 4894–4896.

Mao, L., Rettig, S. J., Thompson, R. C., Trotter, J. & Xia, S. (1996). *Can. J. Chem.* **74**, 433–444.

Masih, D., Chernikova, V., Shekhah, O., Eddaoudi, M. & Mohammed, O. F. (2018). *Appl. Mater. Interfaces*, **10**, 11399–11405.

Maurizot, V., Yoshizawa, M., Kawano, M. & Fujita, M. (2006). *Dalton Trans.* pp. 2750–2756.

Meng, J.-X., Lu, Y., Li, Y.-G., Fu, H. & Wang, E.-B. (2009). *Cryst. Growth Des.* **9**, 4116–4126.

Mirzaei, M., Eshtiagh-Hosseini, H., Alipour, M. & Frontera, A. (2014). *Coord. Chem. Rev.* **275**, 1–18.

Näther, C., Kowallik, P. & Jess, I. (2002). *Acta Cryst.* E**58**, o1253–o1254.

Neels, A., Stoeckli-Evans, H., Wang, Y., Clearfield, A. & Poojary, D. M. (1997). *Inorg. Chem.* **36**, 5406–5408.

Noro, S., Kitagawa, S., Kondo, M. & Seki, K. (2000). *Angew. Chem. Int. Ed.* **39**, 2081–2084.

O'Neal, K. R., Holinsworth, B. S., Chen, Z., Peterson, P. K., Carreiro, K. E., Lee, C., Manson, J. L., Whangbo, M.-H., Li, Z., Liu, Z. & Musfeldt, J. L. (2016). *Inorg. Chem.* **55**, 12172–12178.

Otobe, S., Fujioka, N., Hirano, T., Ishikawa, E., Naruke, H., Fujio, K. & Ito, T. (2015). *Int. J. Mol. Sci.* **16**, 8505–8516.

Podsiadło, M., Jakóbek, K. & Katrusiak, A. (2010). *CrystEngComm*, **12**, 2561–2567.

Premkumar, T., Govindarajan, S., Starosta, W. & Leciejewicz, J. (2004). *Acta Cryst.* E**60**, o1305–o1306.

Ptasiewicz-Bąk, H. & Leciejewicz, J. (1997*a*). *Pol. J. Chem.* **71**, 493–500.

Ptasiewicz-Bąk, H. & Leciejewicz, J. (1997*b*). *Pol. J. Chem.* **71**, 1603–1610.

Ptasiewicz-Bąk, H. & Leciejewicz, J. (1998). *J. Coord. Chem.* **44**, 299–309.

Ptasiewicz-Bąk, H. & Leciejewicz, J. (2003). *J. Coord. Chem.* **56**, 173–180.

Qi, M.-L., Yu, K., Su, Z.-H., Wang, C.-X., Wang, C.-M., Zhou, B.-B. & Zhu, C.-C. (2013). *Dalton Trans.* **42**, 7586–7594.

Rangan, K. K., Trikalitis, P. N. & Kanatzidis, M. G. (2000). *J. Am. Chem. Soc.* **122**, 10230–10231.

Rebek, J. Jr (2005). *Angew. Chem. Int. Ed.* **44**, 2068–2078.

Rodenas, T., Luz, I., Prieto, G., Seoane, B., Miro, H., Corma, A., Kapteijn, F., Llabrés, I., Xamena, F. X. & Gascon, J. (2015). *Nat. Mater.* **14**, 48–55.

Rosen, B. M., Wilson, C. J., Wilson, D. A., Peterca, M., Imam, M. R. & Percec, V. (2009). *Chem. Rev.* **109**, 6275–6540.

Rusbridge, E. K., Peng, Y., Powell, A. K., Robinson, D. & Fitzpatrick, A. J. (2018). *Dalton Trans.* **47**, 7644–7648.

Russell, V. A., Evans, C. C., Li, W. & Ward, M. D. (1997). *Science*, **276**, 575–579.

Sessoli, R., Tsai, H. L., Schake, A. R., Wang, S., Vincent, J. B., Folting, K., Gatteschi, D., Christou, G. & Hendrickson, D. N. (1993). *J. Am. Chem. Soc.* **115**, 1804–1816.

Sha, J., Huang, L., Peng, J., Pang, H., Tian, A., Zhang, P., Chen, Y. & Zhu, M. (2009). *Solid State Sci.* **11**, 417–421.

Shan, S., Tian, Y.-L., Wang, S.-H., Wang, W.-L. & Xu, Y.-L. (2008). *Acta Cryst.* E**64**, o1265.

Shi, F., Li, Z., Kong, L., Xie, Y., Zhang, T. & Xu, W. (2014). *Drug. Discov. Ther.* **8**, 117–120.

Shi, X.-F., Wu, L. & Xing, Z.-Y. (2006). *Acta Cryst.* E**62**, o15–o17.

Shi, X.-F. & Zhang, W.-Q. (2007). *Cryst. Growth Des.* **7**, 595–597.

Singh, M., Kumar, D. & Ramanan, A. (2014). *Proc. Natl Acad. Sci. India A*, **84**, 305–314.

Singh, M., Lofland, S. E., Ramanujachary, K. V. & Ramanan, A. (2010). *Cryst. Growth Des.* **10**, 5105–5112.

Singh, M. & Ramanan, A. (2011). *Cryst. Growth Des.* **11**, 3381–3394.

So, M. C., Wiederrecht, G. P., Mondloch, J. E., Hupp, J. T. & Farha, O. K. (2015). *Chem. Commun.* **51**, 3501–3510.

Souza, M. V. N. de, Lima, C. H. da S., Wardell, J. L., Wardell, S. M. S. V. & Tiekink, E. R. T. (2011). *Acta Cryst.* E**67**, o1714–o1715.

Starosta, W. & Leciejewicz, J. (2010). *Acta Cryst.* E**66**, m744–m745.

Steel, P. J. & Fitchett, C. M. (2008). *Coord. Chem. Rev.* **252**, 990–1006.

Takusagawa, F., Higuchi, T., Shimada, A., Tamura, C. & Sasada, Y. (1974). *Bull. Chem. Soc. Jpn*, **47**, 1409–1413.

Taleghani, S., Mirzaei, M., Eshtiagh-Hosseini, H. & Frontera, A. (2016). *Coord. Chem. Rev.* **309**, 84–106.

Tayebee, R., Amani, V. & Khavasi, H. R. (2008). *Chin. J. Chem.* **26**, 500–504.

Thalladi, V. R., Gehrke, A. & Boese, R. (2000). *New J. Chem.* **24**, 463–470.

Thompson, L. K., Matthews, C. J., Zhao, L., Xu, Z., Miller, D. O., Wilson, C., Leech, M. A., Howard, J. A., Heath, S. L., Whittaker, A. G. & Winpenny, R. E. P. (2001). *J. Solid State Chem.* **159**, 308–320.

Thuéry, P. & Masci, B. (2010). *CrystEngComm*, **12**, 2982–2988.

Tian, A.-X., Ying, J., Peng, J., Sha, J.-Q., Han, Z.-G., Ma, J.-F., Su, Z.-M., Hu, N.-H. & Jia, H.-Q. (2008). *Inorg. Chem.* **47**, 3274–3283.

Tong, M.-L. & Chen, X.-M. (2000). *CrystEngComm*, **2**, 1–5.

Ugalde, M., Gutiérrez-Zorrilla, J. M., Vitoria, P., Luque, A., Wéry, A. S. J. & Román, P. (1997). *Chem. Mater.* **9**, 2869–2875.

Venkatraman, R., Ameera, H., Sitole, L., Ellis, E., Fronczek, F. R. & Valente, E. J. (2009). *J. Chem. Crystallogr.* **39**, 711–718.

Vishweshwar, P., Jagadeesh Babu, N., Nangia, A., Mason, S. A., Puschmann, H., Mondal, R. & Howard, J. A. (2004). *J. Phys. Chem. A*, **108**, 9406–9416.

Vitoria, P., Ugalde, M., Gutiérrez-Zorrilla, J. M., Román, P., Luque, A., San Felices, L. & García-Tojal, J. (2003). *New J. Chem.* **27**, 399–408.

Wang, L., Sun, X.-P., Liu, M.-L., Gao, Y.-Q., Gu, W. & Liu, X. (2008). *J. Cluster Sci.* **19**, 531–542.

Wang, X., Han, N., Lin, H., Luan, J., Tian, A. & Liu, D. (2014). *Inorg. Chem. Commun.* **42**, 10–14.

Wang, X.-L., Hu, H.-L. & Tian, A.-X. (2010). *Cryst. Growth Des.* **10**, 4786–4794.

Wang, X.-L., Liu, D.-N., Lin, H.-Y., Liu, G.-C., Han, N., Luan, J. & Chang, Z.-H. (2015). *RSC Adv.* **5**, 56687–56696.

Wardana, F. Y., Ng, S.-W. & Wibowo, A. C. (2015). *Cryst. Growth Des.* **15**, 5930–5938.

Xiang, G.-Q., Zhu, N.-W., Hu, M.-L., Xiao, H.-P. & Chen, X.-X. (2004). *Acta Cryst.* E**60**, m647–m649.

Yaghi, O. & Li, H. (1996). *J. Am. Chem. Soc.* **118**, 295–296.

Yang, H., Meng, J., Sun, X., Chen, L. & Yang, D. (2014). *Inorg. Chem. Commun.* **39**, 43–46.

Zhang, H., Yu, K., Wang, C., Su, Z., Wang, C., Sun, D., Cai, H., Chen, Z. & Zhou, B. (2014). *Inorg. Chem.* **53**, 12337–12347.

Zhang, L.-Z., An, G.-Y., Yang, M., Li, M.-X. & Zhu, X.-F. (2012). *Inorg. Chem. Commun.* **20**, 37–40.

Zhang, P., Peng, J., Pang, H., Sha, J., Zhu, M., Wang, D., Liu, M. & Su, Z. (2011). *Cryst. Growth Des.* **11**, 2736–2742.

Zhang, S., Zhao, J., Ma, P., Niu, J. & Wang, J. (2012). *Chem. Asian J.* **7**, 966–974.

Zhang, X., Dou, J., Wei, P., Li, D., Li, B., Shi, C. & Hu, B. (2009). *Inorg. Chim. Acta*, **362**, 3325–3332.

Zhang, Y., Fu, X., Zhang, C., Pang, H., Ma, H., Zhao, X. & Wang, C. (2018). *J. Mol. Struct.* **1154**, 543–546.

Zheng, L.-M., Wang, Y., Wang, X., Korp, J. D. & Jacobson, A. J. (2001). *Inorg. Chem.* **40**, 1380–1385.

Zhou, W.-L., Liang, J., Zhao, L., Wang, X.-L., Shao, K.-Z. & Su, Z.-M. (2014). *Inorg. Chem. Commun.* **47**, 48–51.

Zhu, M., Peng, J., Pang, H.-J., Zhang, P.-P., Chen, Y., Wang, D.-D., Liu, M.-G. & Wang, Y.-H. (2010). *Inorg. Chim. Acta*, **363**, 3832–3837.

Zhu, M., Peng, J., Pang, H.-J., Zhang, P.-P., Chen, Y., Wang, D.-D., Liu, M.-G. & Wang, Y.-H. (2011*a*). *Inorg. Chim. Acta*, **370**, 260–264.

Zhu, M., Peng, J., Pang, H.-J., Zhang, P.-P., Chen, Y., Wang, D.-D., Liu, M.-G. & Wang, Y.-H. (2011*b*). *J. Solid State Chem.* **184**, 1070–1078.

Zimmerman, S. C. (1997). *Science*, **276**, 543–544.